Yoshie Endo, Atsumi Sugiyama, Shun-Ai Li, Kazuji Ohmori, Hirokazu Ohata, Yusuke Yoshida, Masabumi Shibuya, Kohji Takei, Masato Enari and Yoichi Taya	Regulation of Clathrin-Mediated Endocytosis by p53.	Genes to Cells	13	375-386	2008

ARTICLE IN PRESS
YDBIO-04221; No. of pages: 15; 4C: 3, 5, 6, 7, 8, 9, 10, 11, 12
Developmental Biology xxx (2009) xxx–xxx
Contents lists available at ScienceDirect
Developmental Biology
journal homepage: www.elsevier.com/developmentalbiology

Brpf1, a subunit of the MOZ histone acetyl transferase complex, maintains expression of anterior and posterior *Hox* genes for proper patterning of craniofacial and caudal skeletons

Kenta Hibiya [a], Takuo Katsumoto [b], Takashi Kondo [c], Issay Kitabayashi [b], Akira Kudo [a,*]

[a] Department of Biological Information, Tokyo Institute of Technology, 4259-B-33 Midori-ku, Nagatsuta, Yokohama 226-8501, Japan
[b] Molecular Oncology Division, National Cancer Center Research Institute, 5-1-1 Tukiji, Chuo-ku, Tokyo, 104-0045, Japan
[c] Kondo Research Unit, Neuro-Developmental Disorder Research Group, Brain Science Institute, Institute of Physical and Chemical Research (RIKEN), 2-1 Hirosawa, Wako, Saitama 351-0198, Japan

ARTICLE INFO

Article history:
Received for publication 10 October 2008
Revised 22 January 2009
Accepted 18 February 2009
Available online xxxx

Keywords:
Brpf1
Moz
TrxG
Medaka
Mutant
bis
Hox
Skeleton
Fin ray

ABSTRACT

The epigenetic mechanism involving chromatin modification plays a critical role in the maintenance of the expression of *Hox* genes. Here, we characterize a mutant of the medaka fish, named *biaxial symmetries* (*bis*), in which *brpf1*, a subunit of the MOZ histone acetyl transferase (HAT) complex, is mutated. The *bis* mutant displayed patterning defects both in the anterior–posterior axis of the craniofacial skeleton and the dorsal–ventral axis of the caudal one. In the anterior region, the *bis* mutant exhibited craniofacial cartilage homeosis. The expression of *Hox* genes was decreased in the pharyngeal arches, suggesting that the pharyngeal segmental identities were altered in the *bis* mutant. In the posterior region, the *bis* mutant exhibited abnormal patterning of the caudal skeleton, which ectopically formed at the dorsal side of the caudal fin. The expression of *Zic* genes was decreased at the posterior region, suggesting that the dorsal–ventral axis formation of the posterior trunk was disrupted in the *bis* mutant. We also found that the MOZ-deficient mice exhibited an abnormal patterning of their craniofacial and cervical skeletons and a decrease of Hox transcripts. We propose a common role of the MOZ HAT complex in vertebrates, a complex which is required for the proper patterning for skeletal development.

Introduction

Determination of 3 axes, i.e., the anterior–posterior (A–P) axis, dorsal–ventral (D–V) axis, and left–right (L–R) axis, underlies the developmental processes of a vertebrate embryo as it forms from the fertilized egg to achieve the proper morphology (Beddington and Robertson, 1999; Kuratani, 2005). The A–P axis is governed by *Hox* genes, which encode homeodomain-containing transcription factors. *Hox* genes were first described in *Drosophila* for their ability to cause segmental homeotic transformation in the body plan (Lewis, 1978; Wellik, 2007). A co-linear relationship exists between the relative orders of *Hox* genes. Genes at the 3′ end of the Hox clusters are activated first in the most-anterior parts of the developing embryo, whereas genes located at the more 5′ genomic position of the Hox clusters are activated subsequently in the more posterior parts (Frohman et al., 1993; Kmita and Duboule, 2003; Kondo and Duboule, 1999). The existence of a 'Hox code' has been proposed to assign morphologies to each segment as a result of the combination of the expression of each *Hox* gene (Kuratani, 2005; Wellik, 2007).

Anteriorly, the craniofacial skeleton is derived from the head segmented pharyngeal arch, the fate of which is determined by *Hox* genes located at the 3′ end of the chromosome (Piotrowski and Nusslein-Volhard, 2000). For instance, targeted inactivation of Hoxa2 in mice causes homeotic transformation of the second arch to the skeletal element derived from the first arch with reverse polarity (Gendron-Maguire et al., 1993; Rancourt et al., 1995; Santagati et al., 2005). Posteriorly, the fate of the skeletal identity in the tail region is determined by *Hox* genes located at the 5′ end of the chromosome (Wellik and Capecchi, 2003). Targeted disruption of Hox13 groups results in an anterior shift of morphology of the vertebrae (Dolle et al., 1993; Economides et al., 2003; Godwin and Capecchi, 1998). Thus, the proper regulation of *Hox* genes is required for the proper morphology along the A–P axis.

The expression of *Hox* genes is regulated in dual phases: an early phase, in which the initial expression pattern of *Hox* genes is established along the A–P axis, and a late phase, in which the expression pattern is sustained during further development (Deschamps et al., 1999; Deschamps and van Nes, 2005). The initiation of the expression of *Hox* genes depends on fibroblast growth factor (Fgf) and retinoic acid (RA) signals, and the counter gradients of Fgf and RA signals control the A–P axis formation via regulation of the expression of these *Hox* genes (Bel-Vialar et al., 2002; Deschamps and

* Corresponding author. Fax: +81 45 924 5718.
E-mail address: akudo@bio.titech.ac.jp (A. Kudo).

0012-1606/$ – see front matter © 2009 Elsevier Inc. All rights reserved.
doi:10.1016/j.ydbio.2009.02.021

van Nes, 2005; Diez del Corral and Storey, 2004). Maintenance of stable expression patterns of the *Hox* genes is regulated by the *Polycomb*-group (PcG) and *Trithorax* group (TrxG) of proteins, which are involved in the epigenetic mechanism via modulating the chromatin structure. Previous reports have demonstrated that PcG proteins repress the expression of *Hox* genes, whereas TrxG proteins maintain the active state of their expression (Papp and Muller, 2006; Soshnikova and Duboule, 2008). In mammals, targeted disruption of PcG genes; *bmi*, *mel-18*, *m33*, and *rae28*, causes an anterior shift of the expression of *Hox* genes, which results in the homeotic transformation of vertebrae to posterior segmental identities (Akasaka et al., 1996; Akasaka et al., 2001; Core et al., 1997; del Mar Lorente et al., 2000; Suzuki et al., 2002; Takihara et al., 1997). Targeted disruption of a mammalian *trx* gene, *mll* in mice, causes a gradual reduction in the expression of *Hox* genes during development (Glaser et al., 2006; Yu et al., 1998, 1995). In addition, a histone acetyltransferase (HAT) of the MYST family, Moz (Myst3), which has been implicated to act as a TrxG, is required for the maintenance of the expression of *Hox* genes in the pharyngeal arches during zebrafish embryogenesis (Miller et al., 2004). Although these studies on PcG and TrxG genes have shown several alterations of *Hox* gene expression in restricted regions of developing embryos, PcG and TrxG functions in the transcriptional regulation of *Hox* genes, especially TrxG functions, have not been adequately demonstrated.

In this study, we isolated and characterized a mutant in medaka named *biaxial symmetries* (*bis*), a mutant which displays patterning defects not only in the A–P axis of its craniofacial skeleton but also in the D–V axis of its caudal fin. In the *bis* mutant, the craniofacial skeleton was homeotically transformed into one with anterior morphology. The expression of *Hox* genes was decreased in the pharyngeal arches in the *bis* mutant, suggesting that the segmental identities of pharyngeal arches had been disrupted. Positional cloning revealed a loss of Brpf1 function in the *bis* mutant. Brpf1, containing a bromodomain and PHD finger, is a TrxG member and a close partner of the MOZ HAT complex (Doyon et al., 2006; Rokudai et al., 2009). This study revealed that Brpf1 is essential for the maintenance of expression of *Hox* genes not only in the anterior region, but also in the posterior region. In the posterior trunk, disruption of Brpf1 function caused decreased expression of *Zic* genes, which regulate the D–V axis of the caudal fin. Furthermore, we characterized the skeletal abnormality of the MOZ-deficient mice, and demonstrated similar abnormalities between the *brpf1* medaka mutant and MOZ-deficient mice, thus implying a common role of the MOZ HAT complex in the skeletal patterning of vertebrates.

Methods

Medaka strains and mutant screening

The medaka (*Oryzias latipes*) strain Cab was used for all studies as the wild type. The *Da* mutant was purchased from local pet shops. The fish were maintained in an aquarium system with re-circulating water at 28.5 °C. Naturally spawned embryos were obtained, incubated at 28 °C, and staged as previously described (Iwamatsu, 2004). Eggs were maintained in the medaka Ringer's solution (0.65% NaCl, 0.04% KCl, 0.011% CaCl2, 0.01% $MgSO_4$, 0.01% $NaHCO_3$, 0.0001% methylene blue).

Mutagenesis using N-ethyl-N-nitrosourea (ENU) was performed according to a standard protocol established for zebrafish (Mullins et al., 1994; Solnica-Krezel et al., 1994; van Eeden et al., 1999), with some modifications (Tanaka et al., 2004). The male fish were exposed to 2.5 or 3 mM ENU for 2 h at room temperature in a buffer containing 0.03% instant ocean (Tetra) and 1 mM sodium phosphate buffer at pH 6.5. The ENU treatment was repeated at 7 days after the initial treatment. Three weeks after the second ENU treatment, these male fish were crossed with the wild-type females to produce families of F1 fish. The F1 fish were then mated to each other to obtain F2 families. For each F2 family, random crosses (up to 8 pairs) were made to obtain the F3 progeny. Embryos and larvae were observed for their mutant phenotypes under a stereomicroscope at 3 different stages (3, 5–6, and 9–10 days after fertilization).

Whole-mount RNA in situ hybridization and skeletal staining

Whole-mount RNA *in situ* hybridization using digoxigenin-labeled anti-sense RNA probes was performed as previously described (Inohaya et al., 1995, 1999). For cartilage staining with Alcian blue 8GX (Sigma), larvae were fixed with 4% paraformaldehyde (Sigma) in PBS at 4 °C overnight, washed twice in PBS containing 0.1% Tween (PBST) for 10 min, and stained with the Alcian blue solution (70% ethanol, 30% acetic acid containing 0.1% Alcian blue) at room temperature overnight. Larvae were hydrated by passage through a graded series of PBS and decolorized in a solution of 1% KOH and 0.9% hydrogen peroxide. Then the larvae were treated at room temperature for less than 1 h with 0.1% trypsin (DIFCO) in a 30% sodium borate saturated solution. The calcified bone was stained with Alizarin red S (Nacalai Tesque). For this staining, larvae were fixed in 4% paraformaldehyde with 0.05 N sodium hydroxide at 4 °C overnight. After a brief washing in PBST, the fixed larvae were stained by immersion in the Alizarin red solution (4% Alizarin red, 0.5% potassium hydroxide) at room temperature for several hours or overnight. Stained samples were stored in 80% glycerol and photographed. For visualization of the cartilage in whole mouse embryos (E14.5), embryos were fixed in 95% ethanol overnight and stained with Alcian blue solution (80% ethanol, 20% acetic acid containing 0.1% Alcian blue) for 24 h. They were then washed for 24 h in 95% ethanol. Cartilages were cleared with 1% KOH. Embryos were stored in 80% glycerol/1% KOH.

Positional cloning

The *bis* heterozygous fish maintained on the southern Cab genomic background were mated with the wild-type northern HNI fish to generate F1 families. Embryos for the genetic mapping were obtained from inter-crosses of the F1 *bis* carriers. For establishment of the initial genetic linkage, bulk segregant analysis was conducted on pools of genomic DNA from the *bis* mutants and wild-type embryos by using the sequence-tagged site (STS) markers on the medaka genome (Kimura et al., 2004). The genetic interval was narrowed down by the analysis of individual embryos by the use of additional STS markers, MF01SSA007H10 and MF01SSA044E03 (Naruse et al., 2000), and newly designed restriction fragment length polymorphism (RFLP) markers, CRELD and BICD2 [CRELD, 5′-AGATAGAAGAC-CAAGTGGAGACG-3′ and 5′-GTATCCTGGATCGCAGATGC-3′/HinfI; and BICD2, 5′-TCTGCGGACAGTCCTAAAGG-3′ and 5′-TTGGACAGAG-CAATCTCAGC-3′/HhaI]. cDNAs of *brpf1* from the *bis* mutants and the wild types were amplified in 2 groups of about 2000 base pairs (bps) and the sequences verified. To directly confirm the linkage between the *bis* locus and *brpf1*, we amplified a part of *brpf1* genomic DNA (primers 5′-GCTAAGGACACGGTGTTTTAC-3′ and 5′-GCTGCCTGGTAC-CATCTGTC-3′), and digested the PCR fragments with the restriction enzyme DdeI, which cleaves the mutant-type allele, but not the wild-type one. The nucleic acid sequence of medaka *brpf1* was deposited in the DDBJ/EMBL/GenBank. Accession No. AB488461.

Immunohistochemistry

Embryos were fixed with 4% paraformaldehyde/PBS for 2 h. After fixation, embryos were washed three times for 10 min each time with MABT (0.1% Triton-X-100 in MAB, which was 100 mM maleic acid and 150 mM NaCl, pH 7.5) and subsequently with MABDT (1% BSA and 1% DMSO in MABT) twice for 30 min each time. After having been blocked with 2% lamb serum in MABDT, embryos were incubated in the blocking solution containing the primary antibody (1:200; anti-Phospho-histone H3; Upstate) overnight at 4 °C. Embryos were

Please cite this article as: Hibiya, K., et al., Brpf1, a subunit of the MOZ histone acetyl transferase complex, maintains expression of anterior and posterior *Hox* genes for prope.... Dev. Biol. (2009), doi:10.1016/j.ydbio.2009.02.021

washed with MABDT three times for 5 min each time, four times for 30 min each time with 2% lamb serum in MABDT for blocking. Thereafter, embryos were incubated with the secondary antibody (1:1000; Alexa-488 conjugated anti-rabbit IgG; Molecular Probes) overnight at 4 °C. Then, embryos were washed with MABT and observed using a confocal microscope (Fluoview FV1000, Olympus).

Generation of construct and transgenic lines

A genomic fragment containing the *brpf1* promoter and Brpf1 coding sequence was amplified in 2 parts (5′ half and 3′ half fragments) from a BAC clone (ola148H10) by using the appropriate primers. The amplified fragments were cloned into the TA cloning vector. We then digested the 5′-half fragment with SalI and NotI, and subcloned it into the XhoI/NotI sites of an I-SceI backbone vector, which contains two I-SceI sites (Thermes et al., 2002). The 3′-half fragment, digested with NcoI and NotI, was cloned into the NcoI site of the inserted 5′-half fragment and the NotI site of the vector. This plasmid was digested with I-SceI (New England Biolabs), and the fragments (20 ng/μl) were injected into the cytoplasm of 1-cell stage embryos. The embryos showing a transiently strong expression of the exogenous gene were allowed to grow to adulthood. We then checked the GFP expression in the next generation, and picked an embryo with stable integration of the injected construct as the transgenic line.

Determination of the genotype of the rescued *bis* mutant was performed by using ENU-induced polymorphism, which exists at the genomic region 70 kb separated from the *brpf1* mutation point. This polymorphism showed strong linkage with the *brpf1* mutation (0 recombinations per 980 meioses). It was difficult to use the *brpf1* mutation point itself for determining the genotype because of the rescue construct containing the wild-type *brpf1* sequence. The genomic fragment was amplified by using the following primers: forward, 5′-ACTTCTTCTGCTTCACATGTGAC-3′, and reverse, 5′-AGAGA-CAGTCCTGGTATTCGG-3′, and sequenced by means of direct sequencing for determination of the genotype.

Whole-mount in situ hybridization of mouse embryos

Whole-mount *in situ* hybridizations were carried out according to the established protocol (Kondo and Duboule, 1999), using DIG-labeled riboprobes. Embryos were permeabilized with 10 μg/ml proteinase K for 15 min. Probes (*Hoxa3* (Manley et al., 2004), *Hoxa4* (Kawazoe et al., 2002), *Hoxd10* (Renucci et al., 1992), *Hoxd11* (Izpisua-Belmonte et al., 1991)) were described previously.

Results

Isolation of a medaka mutant that exhibits pharyngeal cartilage homeosis

To investigate organogenesis of vertebrates, we performed a medium-scale screening of medaka mutants obtained by ENU

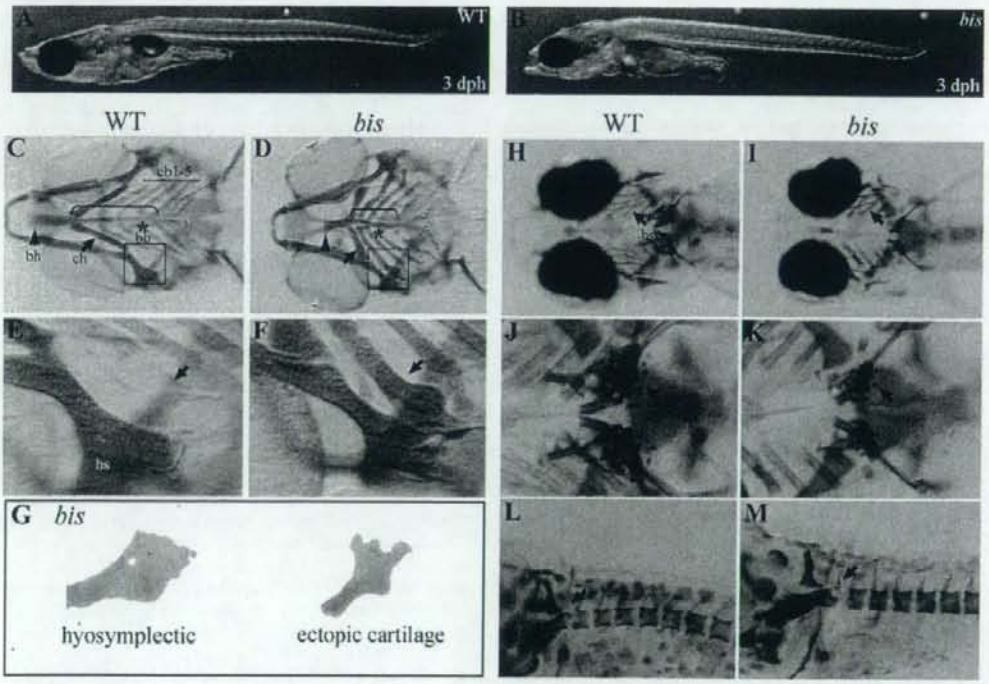

Fig. 1. The *bis* mutant displayed skeletal malformation. (A, B) Lateral view of a 3 dph larva. The *bis* mutant has a shrunken head. Other tissues appeared to have a normal morphology. (C–G) Craniofacial cartilage stained with Alcian blue. (C, D) Ventral view of wild-type and *bis* larvae. The bracket indicates the head region of the *bis* mutant and wild-type. Arrowheads indicate basihyal, which is decreased in the *bis* mutant; and arrows, the ceratohyal, which is short and thick in the mutant. (E, F) Highly magnified view of black boxed region in "C" and "D". The arrow in "F" indicates the ectopic cartilage at the lateral end of the first ceratobranchial in the *bis* mutant, compared with the wild-type (arrow in "E"). (G) View of a flat-mounted hyosymplectic and the ectopic cartilage of the *bis* mutant. The shape of ectopic cartilage has features characteristic of the hyosymplectic. (H–M) Calcified bone was stained with Alizarin red. (H, I) Ventral view of the wild type and the *bis* mutant. Arrows indicate the branchiostegal rays, which are decreased in number in the *bis* mutant. (J, K) Highly magnified view of the tooth region. Arrows indicate this region, where small pharyngeal teeth are seen in the *bis* mutant. (L, M) Lateral–dorsal view of the neck region. Arrows indicate the first vertebra, which is fused to the head in the *bis* mutant. bh, basihyal; ch, ceratohyal; cb 1–5, first to fifth ceratobranchial; bb, basibranchial; hs, hyosymplectic; bsr, branchiostegal ray; pt, pharyngeal tooth.

Please cite this article as: Hibiya, K., et al., Brpf1, a subunit of the MOZ histone acetyl transferase complex, maintains expression of anterior and posterior *Hox* genes for prope.... Dev. Biol. (2009), doi:10.1016/j.ydbio.2009.02.021

mutagenesis, and isolated the medaka mutant *biaxial symmetry* (*bis*). The *bis* mutant dies several days after hatching. Morphological examination showed the *bis* mutant to have a shrunken head (Figs. 1A, B). To visualize the craniofacial skeleton, we stained medaka larvae at 3 days post hatching (dph) with Alcian blue for cartilage. The craniofacial cartilage of the *bis* mutant was shrunk compared with that of the wild-type larvae (Figs. 1C, D). In the *bis* mutant, the length of each gill cartilage (ceratobranchials) was shorter, and the basihyal (derived from the second pharyngeal arch) was shortened compared with that of the wild-type larva (Figs. 1C, D, arrowhead and brackets). The ceratohyal (derived from the second pharyngeal arch) was shorter and thicker than that of the wild type (Figs. 1C, D, arrow). The second to the fifth ceratobranchials in the *bis* mutant were thicker and longer than those in the wild-type larvae (Figs. 1C, D). Although the basibranchial was separated in 2 parts in the wild-type larvae at the third ceratobranchial, the basibranchial was fused and extended to the fifth ceratobranchial in the *bis* mutant (Figs. 1C, D, asterisk). In addition, an ectopic cartilage was detected at the lateral end of the first ceratobranchial (derived from the third pharyngeal arch) on both sides of the head (Figs. 1C, D, square; E, F, arrow). An ectopic cartilage was often observed at the lateral end of the second ceratobranchial (Figs. 1C, D and Table 1). To further characterize the abnormalities of the *bis* mutant, we focused on the shape of the ectopic cartilage at the lateral end of the first ceratobranchial in the *bis* mutant. A flat-mounted observation revealed that the shape of the ectopic cartilage had the characteristic feature of the hyosymplectic, which is normally derived from the second pharyngeal arch (Fig. 1G). To observe the calcified bone, we stained the larvae with Alizarin red. Deformed brachiostegal rays (Figs. 1H, I arrow) and small pharyngeal teeth (Figs. 1J, K, arrow) were observed in the *bis* mutant. In the cervical region, the vertebra with neural arch was fused to the head skeleton in the *bis* mutant (Figs. 1L, M arrow). These results indicate that the *bis* mutant exhibits patterning abnormality of its craniofacial skeleton, suggesting that the pharyngeal segmental identity in the *bis* mutant had been disrupted.

Table 1
Skeletal phenotype of the *bis* mutant.

Cranio facial cartilage	n = 83
Arch2	
Basihyal reduced	83 (100%)
Ceratohyal shorter and thicker	83 (100%)
Arch3	
Ectopic cartilage at the lateral end of 1st cb	83 (100%)
Ectopic cartilage shape	
Small fragment	5 (6.0%)
Simple stick shape	16 (19.2%)
Similar to hs	62 (74.7%)
Hyobranchials absent	83 (100%)
Posterior arch	
Ectopic cartilage at the lateral end of 2nd cb	17 (20.4%)
Hyobranchials absent	83 (100%)
Ceratobranchials distally broadened	83 (100%)
Cervical and pharyngeal bone	n = 32
Fused vertebrate to head bone	28 (87%)
Reduced pharyngeal tooth	32 (100%)
Caudal skeleton	n = 50
Fused vertebrae	38 (76%)
Extra vertebra at the end of notochord	46 (90%)
Dorsally formed fin rays	50 (100%)
Reduced hypurals	43 (86%)

Percentage of animals with each phenotype was listed. Phenotypes of craniofacial cartilages were assessed by Alcian blue staining at 3 dph. Phenotypes of cervical and pharyngeal bone were assessed by Alizarin red staining at 3 dph and those of caudal skeletons were assessed by Alizarin red staining at 4 dph. These phenotypic differences of caudal skeleton were most likely caused by the subtle difference of the developmental stage in each animal.

The bis mutant exhibits defective skeletal patterning at the posterior region

The *bis* mutant exhibited disruption of the skeletal patterning not only in the anterior head region, but also in the posterior region. Compared with those of the wild-type larvae, the fin rays were ectopically formed at the dorsal region of caudal fin in the mutant (Figs. 2A, B, arrow); and the ossification pattern was disrupted at the caudal vertebrae in the *bis* mutant. An extra vertebra had formed at the end of the notochord in the *bis* mutant (Figs. 2A, B, arrowhead). In addition, the ossified hypural in the *bis* mutant was smaller than that of the wild type, and the hypural of the caudal most vertebra was deleted in the *bis* mutant (Figs. 2A, B, asterisk). Morphological analyses of embryos stained with Alcian blue revealed that the hypural was also ectopically formed at the dorsal side of the caudal fin and that each hypural was fused in the *bis* mutant (Figs. 2C, D, arrow). Furthermore, the blood vessels were ectopically extended at the dorsal side of the caudal fin in the *bis* mutant at 7 dpf (Fig. 2F, arrow) as opposed to their normal pattern in the wild type (Fig. 2E, arrow). To further characterize the caudal 287 fin abnormality of the bis mutant, we examined mitotic cells using mitotic marker phospho-histone H3 antibody at day 7 post fertilization (7 dpf), because the mesenchyme of the caudal fin, which exists at the ventral caudal end of the notochord, is known highly proliferative and involved in the development of the caudal fin (Hadzhiev et al., 2007; Sakaguchi et al., 2006). In the wild-type larvae, the mitotic cells largely existed at the ventral caudal end of the notochord (Fig. 2 arrow in G, I), as reported previously (Hadzhiev et al., 2007; Sakaguchi et al., 2006); whereas in the *bis* mutant, the mitotic cells existed not only at the ventral caudal end of the notochord but also at the dorsal caudal end (Fig. 2 arrow in H, I). These results indicate that the *bis* mutant exhibits a defect in the dorsal–ventral patterning of caudal fin.

The bis locus encodes brpf1

To identify a genomic mutation in the *bis* mutant, we mapped the mutated genomic position on the genetic linkage map by using the sequence-tagged site (STS) markers, and subsequently mapped it to within 0.1 cM distance in Linkage Group 7 (1 recombination among 980 meioses in Fig. 3A; see Methods). By searching for genes and ESTs that have been previously mapped to this genomic region, we found 3 predicted genes homologous to *fgd1*, *wnk*, and *brpf1*. We then sequenced the RT-PCR fragment of these candidate genes from *bis* and wild-type embryos, and found a T to A nonsense mutation in the open reading frame of *brpf1* cDNA (Fig. 3B). Using both the alignment of vertebrate Brpf1 amino acid sequences and the 5′ and 3′ race methods, we identified the medaka full-length *brpf1* cDNA sequence, which encoded 5451 bp and a 1283 amino acid protein with a high similarity to the mammalian Brpf1 (68% identical to human and mouse Brpf1) and zebrafish Brpf1 (77% identical to zebrafish one). In the medaka genome sequence, we could not find other paralogues of Brpf1. Brpf1 contains a BROMO domain, which has a binding affinity for the acetylated lysine of histones (Dhalluin et al., 1999; Yang, 2004); a PHD domain, which has a binding affinity for tri-methylated lysine of histones (Pena et al., 2006; Taverna et al., 2006); and a PWWP domain, which has affinity for condensed chromosomes (Laue et al., 2008; Turlure et al., 2006). In the *bis* mutant, the T to A transition introduced a stop codon (Y810Stop) at the end of BROMO domain, resulting in a truncated form of Brpf1 (Figs. 3B, C).

To examine the expression pattern of *brpf1*, we performed whole-mount RNA *in situ* hybridization on medaka embryos. The expression of *brpf1* was ubiquitous at st 21 (Fig. 3D), whereas at st 30 it was decreased in the trunk region and expressed in the

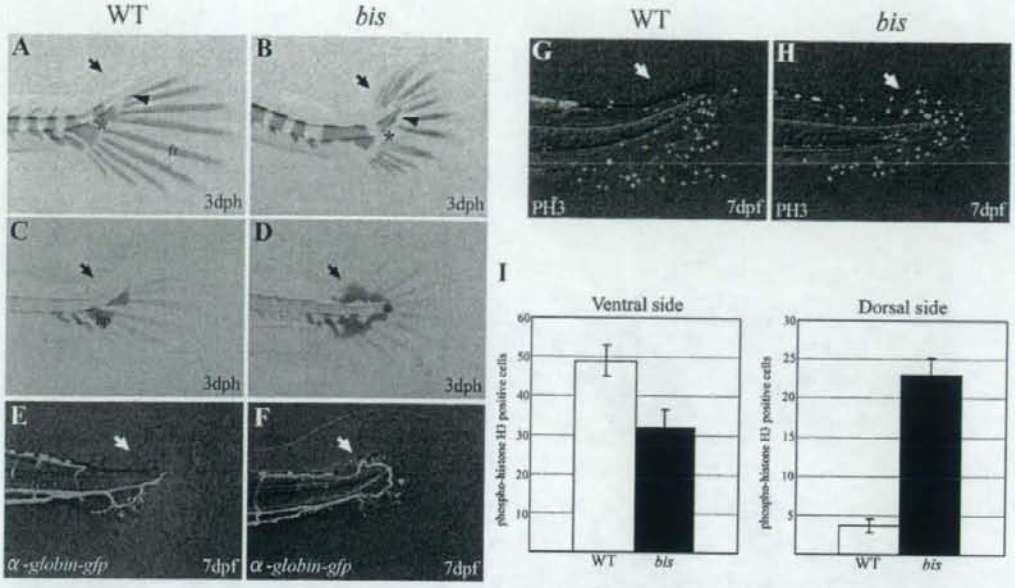

Fig. 2. The *bis* mutant exhibits D–V axis disruption in its caudal region. (A, B) Calcified bone of the caudal fin was stained with Alizarin red. A lateral view of the wild type and the *bis* mutant is shown. The arrow in "B" indicates the ectopic formation of fin rays at the dorsal region in the *bis* mutant; and that in "A" denotes its absence. The arrowhead in "B" indicates the abnormal patterning of the vertebra formed at the tip of the notochord, whereas that in "A" shows the normal patterning. In "B", the asterisk denotes the reduced or absence of hypurals in the *bis* mutant; and that in "A", the normal hypurals. (C, D) Cartilage of the caudal fin was stained with Alcian blue. A lateral view of the wild type and the *bis* mutant is shown. The arrow in "D" indicates the ectopic formation of the hypural cartilage at the dorsal side in the *bis* mutant, compared with the wild-type (arrow in "C"). (E, F) Blood vessels are visualized in the α-*globin*-GFP transgenic medaka. The blood vessel has ectopically extended at the dorsal side of the notochord in the mutant (F, arrow); and its absence there is indicated by the arrow in "E". (G, H) Mitotic cells were labeled with anti-phospho-histone H3 antibody. A lateral view of the caudal fin is shown. The arrow in "H" points to the ectopic proliferating cells at the dorsal side of the caudal region in the *bis* mutant, compared with the wild-type (arrow in "G"). (I) Histogram showing that mitotic cells were significantly increased at the dorsal side in the *bis* mutant. Error bar indicate S.D. fr, fin ray; hp, hypural.

pharyngeal arches and neural epithelium (Fig. 3E, arrow and arrowhead). The expression of *brpf1* was strong in the head region; however, the expression of *brpf1* was also detectable in the trunk and caudal region by long exposure at 4 dpf (Figs. 3F, G). In the *bis* mutant, *brpf1* mRNA could be detected, suggesting that the *bis* mutation does not affect the stability of *brpf1* mRNA and that the *bis* mutant produces truncated Brpf1 protein (Figs. 3H, I). In the *bis* mutant, the expression of *brpf1* mRNA existed, we then examined how this mutation affects the Brpf1 function by observing in vitro interaction with other members of the MOZ HAT complex and cellular localization of Brpf1. We generated the HA tagged human Brpf1 construct which contains the stop codon at the corresponding site to the *bis* mutation. By the *bis* mutation, the PWWP domain was deleted. Recently, it was demonstrated that the PWWP domain was not required for the interaction with Moz and Ing5 (Ullah et al., 2008). Consistent with this report, the truncated Brpf1 was normally interacted with Moz and Ing5 (Supplementary Figs. 1A–C). Although the truncated Brpf1 could be interacted with other members of the MOZ HAT complex, truncated Brpf1 was not co-localized with the condensed chromosome of mitotic cells (Supplementary Fig. 1D) as described previously (Laue et al., 2008; Turlure et al., 2006). These data suggest that the *bis* mutation causes the defect of Brpf1 function.

brpf1 is the gene responsible for the bis mutant

To confirm that the defects in the *bis* mutant were due to the genomic mutation in the *brpf1* gene, we rescued the *bis* mutant by introducing into the *bis* mutant the wild-type *brpf1* gene under the control of the genomic *brpf1* promoter region. To express the wild-type *brpf1* in an appropriate position and stage, we first obtained a genomic DNA fragment involving the 6-kb upstream region from the first methionine codon of the *brpf1* gene by the PCR. To check the ability of this promoter region to express the *brpf1* gene, we constructed an EGFP reporter vector and generated transgenic medaka. Fluorescent signals of EGFP were similar to the expression pattern of endogenous *brpf1* mRNA (Figs. 3J, K), suggesting the suitability of this 6-kb promoter region. We then generated a transgenic construct that contained the 6-kb promoter region, the genomic sequence encoding the *brpf1* gene, and the *crystalin* promoter-GFP that is used for checking the transgene integration into a chromosome (the construct is shown in Fig. 4A). We micro-injected the rescue DNA construct into the fertilized eggs of heterogenous mutants, picked up embryos with EGFP-positive eyes, and then inter-crossed the offspring to obtain the *bis* mutant harboring the rescue DNA construct. The *bis* mutant that had the rescue DNA construct developed normally, and was indistinguishable from the wild type. Histomorphometric analyses using Alcian blue and Alizarin red showed that the skeletal patterning of the rescued *bis* mutant indicated a restored normal morphology (Figs. 4B–J). These results confirm that the *brpf1* gene was responsible for the *bis* mutant.

Brpf1 is required for the maintenance of expression of Hox genes

The defect in the segment patterning along the A–P axis in the *bis* mutant implies that the faulty regulation of *Hox* gene expression by the chromatin structure (known as TrxG and PcG) is responsible for the *bis* mutant phenotypes, because Brpf1 is a component of the MOZ HAT complex (Doyon et al., 2006). To elucidate the involvement

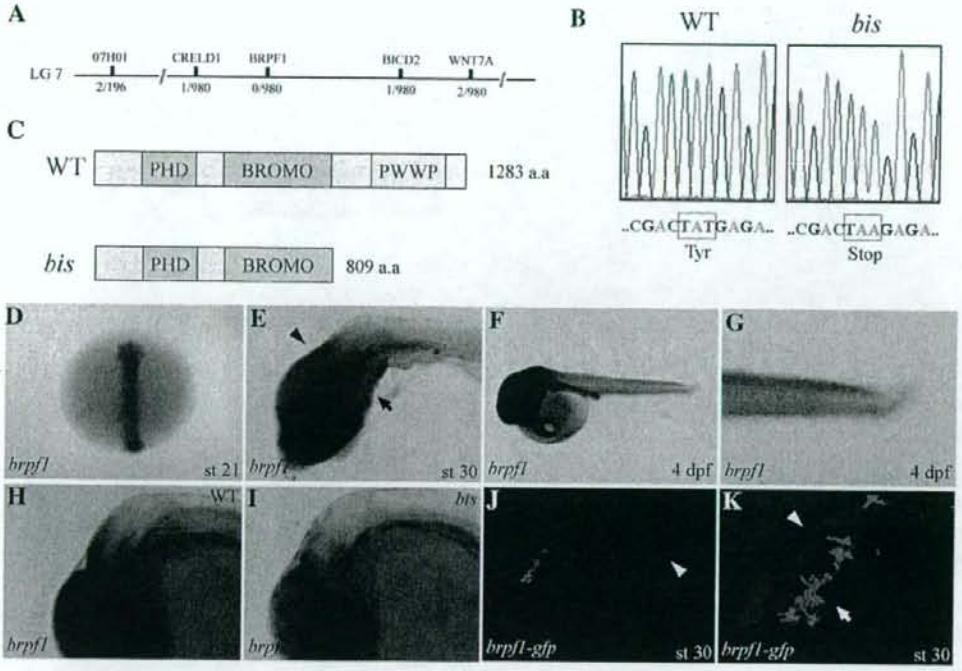

Fig. 3. The *bis* locus encodes the *brpf1*. (A) Genetic map of the *bis* locus in LG7. The number of recombinations is shown under the line. (B) The *bis* mutant has a T to A non-sense mutation in the *brpf1* gene. (C) Schematic of Brpf1 protein structure in the wild type and the *bis* mutant. The T to A transition results in the Y810Stop and thus generates a truncated Brpf1 protein with the bromo domain as its end in the *bis* mutant. (D–I) The expression pattern of *brpf1*. (D) *brpf1* is expressed ubiquitously at st 21. (E) The expression of *brpf1* became intense in the head at st 30. The arrow and arrowhead indicate the expression of *brpf1* at the pharyngeal arch and hindbrain, respectively. (F, G) The expression of *brpf1* at 4 dpf after long exposure. The expression of *brpf1* is observed in the trunk region and caudal end. (H, I) Lateral view of expression of *brpf1* in the wild type (H) and in the *bis* mutant (I) at st 30. The expression of *brpf1* is normal in the *bis* mutant. (J, K) Confocal microscope images of the *brpf1*-GFP transgenic medaka. The GFP signals are observed to have a pattern similar to that of the endogenous *brpf1* expression (J and K, arrowhead. Compare with the E and F). The intense signal was a non-specific signal due to pigment (arrow in "K").

of *Hox* genes in the *bis* phenotypes, we first examined the expression of *hoxa2a*, *hoxa3a*, *hoxa4a*, *hoxa5a*, *hoxb1a*, *hoxb2a*, *hoxb3a*, *hoxb4a*, and *hoxb5a* in medaka, which were previously reported to be expressed in the pharyngeal arches and involved in the establishment of the A–P axis identity of the pharyngeal arches and hindbrain in mice and zebrafish (Favier and Dolle, 1997; Kimmel et al., 2001). Although the expression of *hoxb1a* was maintained in rhombomere 4 during development of the wild-type at st 29 to st 31 (Supplementary Fig. 2A), the expression gradually decreased in the *bis* mutant (Supplementary Fig. 2B).

Hox2 and 3 group genes play a crucial role in determining the segmental identity at the second and third pharyngeal arches, respectively (Kimmel et al., 2001). We first examined the expression of Hox 3 group in the *bis* mutant, because the ectopic cartilage formation at the third pharyngeal arch implied the disruption of the segmental identity at the third arch in the *bis* mutant. The expression of both *hoxa3a* and *hoxb3a* was severely decreased at this pharyngeal arch and mildly decreased in the hindbrain of the *bis* mutant (Fig. 5A, B arrow and arrowhead in right panels), compared with that in the wild type (Figs. 5A, B arrow and arrowhead in left panels). Notably, the expression at the third pharyngeal arch was most affected and completely abolished in the *bis* mutant (Figs. 5A, B, line). These results suggest that the segmental identity of the third arch had transformed to become another segmental identity in the *bis* mutant. In other *Hox* genes, similar decrease was observed in the *bis* mutant (Supplementary result and Supplementary Figs. 2C, D).

These *Hox* genes were normally expressed in the early stage (st 22–27) in the *bis* mutant (data not shown). These results suggest that Brpf1 is involved in the maintenance of the expression of *Hox* genes in the pharyngeal arches.

The segmental identities are disrupted in the pharyngeal arch in the bis mutant

The maintenance of the expression of *Hox* genes is essential for the establishment of the segmental identity of the pharyngeal arches (Santagati et al., 2005). The segmental identities of pharyngeal arches are defined by the expression of *goosecoid* (*gsc*) and *bapx1*, which are essential for the proper patterning of the craniofacial cartilage (Rivera-Perez et al., 1995; Tucker et al., 2004). To investigate the effects of decreased expression of *Hox* genes on pharyngeal arch identities in the *bis* mutant, we examined the expression of *gsc* and *bapx1* at the late stage (st 30), when the expression of *Hox* genes was severely decreased in the pharyngeal arches in the *bis* mutant. Although *gsc* was expressed in the first and second pharyngeal arches in the wild type, an ectopic expression of gsc was detected in the third and fourth arches in the *bis* mutant (Fig. 5C, arrows in upper panels). The expression of *gsc* in the fifth to seventh pharyngeal arches corresponding to the putative pharyngeal teeth was decreased in the *bis* mutant (Fig. 5C, arrowheads in lower panels), arches which correspond to the putative pharyngeal teeth. The expression of *bapx1* at the pharyngeal arch was also anteriorized in the *bis* mutant (Supplementary result and Supplementary Figs. 3A, B). In mice,

Please cite this article as: Hibiya, K., et al., Brpf1, a subunit of the MOZ histone acetyl transferase complex, maintains expression of anterior and posterior *Hox* genes for prope..., Dev. Biol. (2009), doi: 10.1016/j.ydbio.2009.02.021

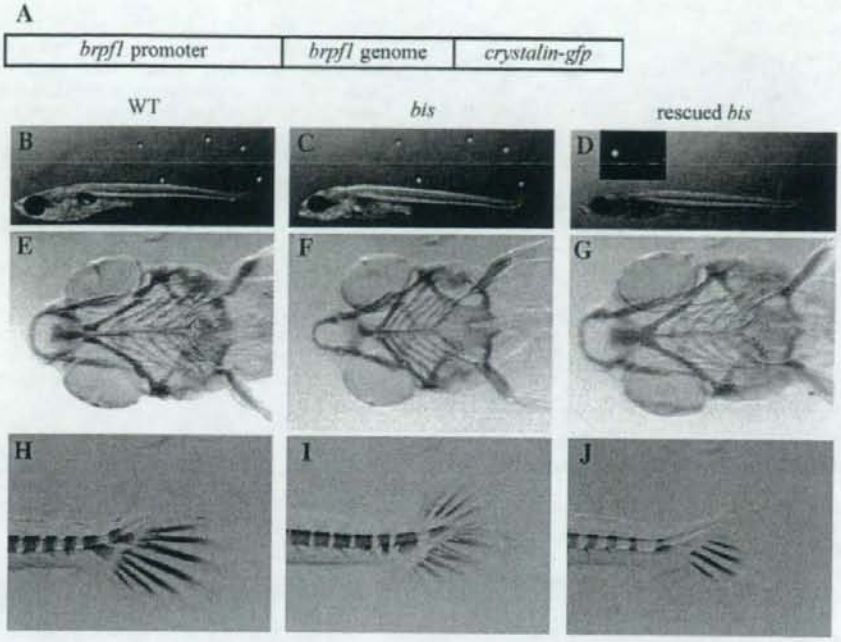

Fig. 4. *brpf1* is responsible gene for the *bis* mutant (A) Schematic of the rescue DNA construct. This construct contains the 6-k *brpf1* promoter, genomic sequence coding for the Brpf1 protein, and *crystalin* promoter-GFP. (B–D) The lateral view of the wild-type (B), *bis* (C), and rescued *bis* larva (D) at 3 dph is shown. Rescue construct-treated *bis* mutants show restoration of the normal morphology. The inset in "D" shows the expression of GFP in lens. (E–G) Ventral view of craniofacial cartilage of the wild type (E), *bis* (F), and rescued *bis* larva (G) stained with Alcian blue. The ectopic cartilage and shrunken gill arches were not observed in the rescued *bis* mutant. (H–J) The lateral view of caudal fin rays of the wild-type (H), *bis* (I), and rescued *bis* (J) larvae stained with Alizarin red. Ectopically formed dorsal fin rays are not observed in the rescued *bis* mutant.

inactivation of *hoxa3* gene results in the defect in thymus formation (Le Douarin and Jotereau, 1975; Manley and Capecchi, 1997, 1998). Then, we investigated *rag1* expression which was expressed in the hematopoietic cells at the thymus (Willett et al., 1997). In the *bis* mutant, *rag1* expression was reduced compared with the wild type (Supplementary result and Supplementary Fig. 3C). These results indicate that the segmental identity of pharyngeal arches was altered to the anterior identity in the *bis* mutant.

Brpf1 is required for the maintenance of Hox gene expression in the posterior region

The decreased expression of *Hox* genes in the anterior region can account for the anterior transformation of the pharyngeal arch in the *bis* mutant, whereas it still remained unclear how this decreased expression would result in the defect in the caudal fin. To clarify the caudal fin phenotype of the *bis* mutant, we focused on the Brpf1 function that is required for the maintenance of the expression of the posterior *Hox* genes. We then investigated the expression of *Hox* genes that are expressed in the caudal trunk region (*hoxa13a*, *hoxc11a*, *hoxc12a*, *hoxc13a*, *hoxd11a* and *hoxd12a*). Although *hoxc11a* was expressed in the caudal trunk in the wild type at 4 to 6 dpf, its expression gradually decreased in the *bis* mutant at 4 to 6 dpf (Fig. 6A). Expression of *hoxc12a* was detected in the caudal trunk region in the wild type. In the *bis* mutant, this expression was decreased at 4 to 6 dpf (Fig. 6B). The *hoxc13a* gene was expressed in the tip of the wild-type tail; whereas, in the *bis* mutant, the expression gradually decreased at 4 to 6 dpf (Fig. 6C). For other *Hox* genes, a similar decrease was observed in the *bis* mutant (Supplementary Figs. 4A–C). Then, to investigate whether Brpf1 has a role in the maintenance of the expression of all *Hox* genes, we examined the expression of *Hox* genes located at the center of the Hox cluster. In the *bis* mutant, the expression of *hoxa9a*, *hoxb6a*, and *hoxb8a* were not affected, and the expression of *hoxb9a* was mildly decreased. On the other hand, the expression of *hoxd10a* was severely decreased in the *bis* mutant (Supplementary Figs. 5A–E). These results suggest that Brpf1 is required for the maintenance of the expression of the anterior and posterior *Hox* genes but not for that of the center *Hox* genes.

The caudal skeletal phenotypes of the bis mutant were similar to those of the double anal fin mutant (Da) in medaka

Posteriorly, the *bis* mutant exhibited the abnormality of D–V axis formation at the caudal fin. Then, we focus on the *Da* mutant which exhibits abnormal D–V axis formation in its somite and epithelial derivatives (Ohtsuka et al., 2004). To elucidate the similarity and difference between phenotypes of the *bis* mutant and those of the *Da* mutant in the caudal tissue, we compared the caudal skeletal abnormalities between the 2 mutants. The phenotype of caudal fin in the *bis* mutant was very similar to that of the *Da* mutant (Figs. 7A, B, arrows; C, D, arrows), implying that a similar mechanism was disrupted in the caudal fin of the *Da* and *bis* mutant. On the other hand, the extra vertebra and fused hypurals were not observed in the *Da* mutant (Figs. 7A, B, arrowheads; C, D). We then elucidated whether the expression of *Hox* genes was affected in the posterior region in the *Da* mutant. Although the expression of *hoxa13a* and *hoxc13a* in the posterior region was severely decreased in the *bis* mutant (Supplementary Fig. 4A and 6C), the expression of these *Hox* genes was normally expressed in the *Da* mutant (Figs. 7E, F). This result suggests that the expression of *Hox* genes is not directly linked with the appropriate D–V axis formation of the caudal fin.

Please cite this article as: Hibiya, K., et al., Brpf1, a subunit of the MOZ histone acetyl transferase complex, maintains expression of anterior and posterior *Hox* genes for prope.... Dev. Biol. (2009), doi:10.1016/j.ydbio.2009.02.021

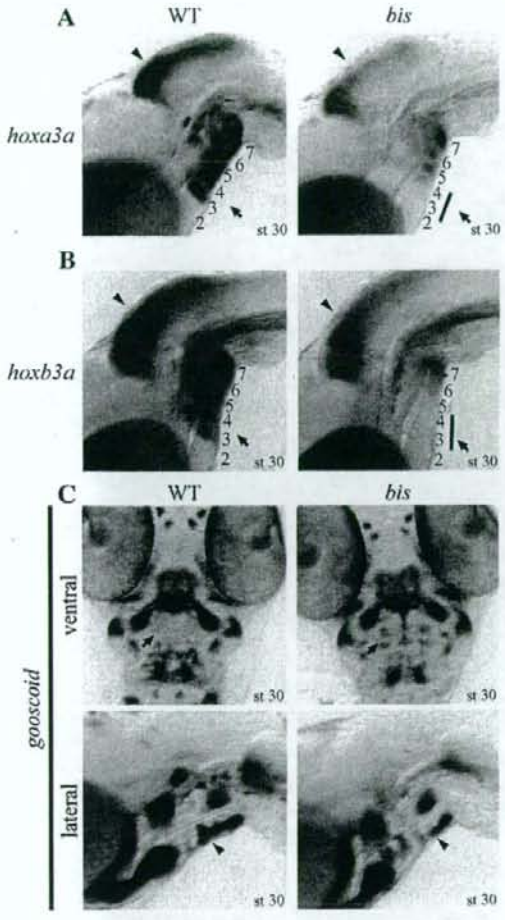

Fig. 5. Brpf1 is essential for the maintenance of expression of *Hox* genes and establishment of identities of pharyngeal arch. Developmental stages are indicated in lower right corners. (A) Expression of *hoxa3a* in the wild type and the *bis* mutant. Arrows indicate the expression, which is decreased in the third and fourth pharyngeal arches. (B) Expression of *hoxb3a* in the wild-type and the *bis* mutant. Arrows indicate the expression, which is reduced in the third and fourth pharyngeal arches. Note that the decrease in the levels of expression of *Hox* genes in the hindbrain was less severe than in those of *Hox* genes in the pharyngeal arches (arrowhead and arrow, respectively, in "A, B"). (C) Upper panels show ventral views and lower panels show lateral views of expression of *goosecoid* (*gsc*) in the wild type and the *bis* mutant. Arrows indicate the expression, which is ectopic in the third and fourth pharyngeal arches in the *bis* mutant. Arrowheads indicate the expression in the fifth to seventh pharyngeal arches, which is decreased in the *bis* mutant.

Expression of Zic genes is decreased in the posterior trunk region of the bis mutant

The *Da* mutant has 2 insertions near the *zic1* and *zic4* genes, resulting in the decreased expression of *zic1* and *zic4* genes at the dorsal somite in the *Da* mutant (Ohtsuka et al., 2004). To investigate the D–V axis formation governed by *Zic* genes in the *bis* mutant, we examined the expression of *zic1* and *zic4* genes in it. The expression of the *zic1* gene gradually decreased in the dorsal neural tube and somatic cells in the *bis* mutant from 4 to 6 dpf, compared with that in the wild type (Figs. 8A, B). The *zic4* gene was also decreased in expression in the *bis* mutant (Fig. 8C, D). Although, in the *bis* mutant, the expressions of *zic1* and *zic4* genes were severely decreased at the caudal tissue, their expressions were not affected in the midbrain, hindbrain and anterior neural tube (Fig. 8E, arrows and arrowheads and data not shown). These results suggest that the disruption of the D–V axis formation at the caudal fin in the *bis* mutant was due to the decreased expression of *Zic* genes in the posterior trunk.

MOZ HAT complex has a common role in the skeletal patterning

In medaka, Brpf1 has a crucial role in the patterning of the anterior and posterior skeletons. We then investigated whether the function of the MOZ HAT complex in the skeletal patterning was common between fishes and mammals. To examine the skeletal abnormality in the Moz−/− mice (Katsumoto et al., 2006), we stained cartilages of E14.5 embryos with Alcian blue. The lesser horn

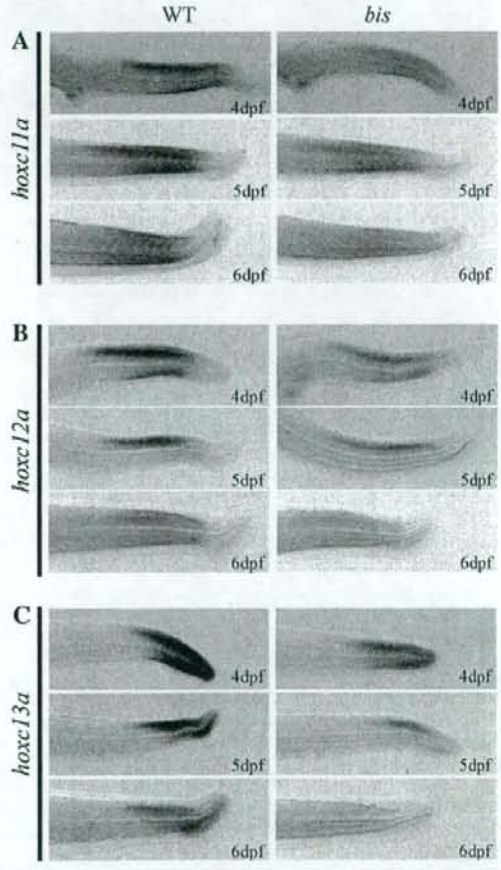

Fig. 6. Brpf1 is required for the regulation of expression of posterior *Hox* genes. Developmental stages of the embryo are indicated in the lower right corners, and lateral views are shown for all photos. (A) Expression of *hoxc11a* in the wild type and the *bis* mutant. The expression of *hoxc11a* gradually decreases in the *bis* mutant. (B) Expression of *hoxc12a* in the wild type and the *bis* mutant. The expression of *hoxc12a* is also decreased in the *bis* mutant. (C) Expression of *hoxc13a* in the wild type and the *bis* mutant. The expression of *hoxc13a* has completely decreased by 6 dpf in the *bis* mutant.

Please cite this article as: Hibiya, K., et al., Brpf1, a subunit of the MOZ histone acetyl transferase complex, maintains expression of anterior and posterior *Hox* genes for prope... Dev. Biol. (2009), doi:10.1016/j.ydbio.2009.02.021

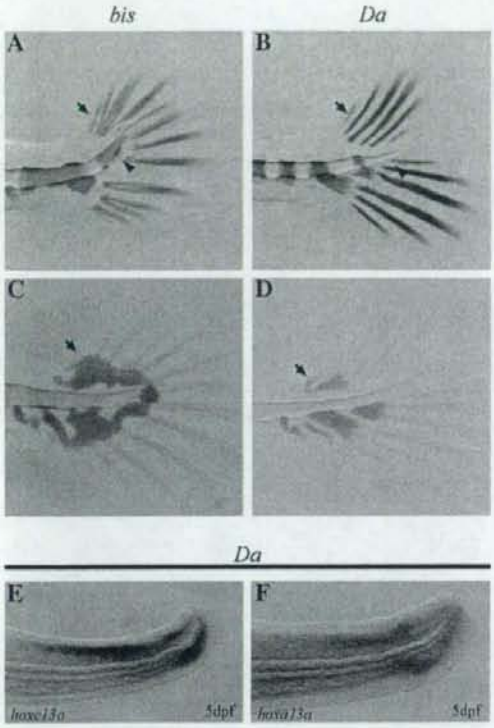

Fig. 7. The *Da* mutant exhibits a caudal fin phenotype similar to that of the *bis* mutant. Lateral views are given for all photos. (A, B) Caudal skeleton stained with Alizarin red at 3 dph. Ectopic dorsal formation of fin rays is evident in both the *bis* mutant and the *Da* mutant (arrow). However, evidence of ectopic formation of vertebrae is not observed in the *Da* mutant (arrowhead), though it is in the *bis* one (arrowhead). (C, D) Cartilage stained with Alcian blue at 3 dph. Evidence of ectopic dorsal formation of hypurals is seen in both the *bis* mutant (arrow) and the *Da* mutant (arrow). However, the fused hypurals are not observed in the *Da* mutant. (E) Expression of *hoxc13a* in the *Da* mutant. (F) Expression of *hoxa13a* in the *Da* mutant. The expression of *hoxc13a* and *hoxa13a* is normal in the *Da* mutant.

of the hyoid is derived from the second pharyngeal arch; and the greater horn, from the third pharyngeal arch. Moreover, the hyoid body is derived from the second and third pharyngeal arches (Lumsden et al., 1991; Noden, 1978, 1988). In the ventral view of hyoid cartilage, the shape of the hyoid body was changed rostrally to an acute shape in the Moz−/− mice (Figs. 9A–G); and in the anterior view, the lesser horn of hyoid was seen to have fused to the hyoid body in the Moz−/− mice (Figs. 9C, D, G). In the dorsal–lateral view, an accessory projection was observed on the greater horn of the hyoid in the Moz−/− mice (Figs. 9E, F, G). Although in the Moz−/− mice, a small ectopic cartilage was formed adjacent to the styloid process, other structures derived from the second pharyngeal arch were not affected in the Moz−/− mice (Supplementary Figs. 7A–D). In the *bis* mutant, the first cervical vertebra was fused to the head skeleton. So we examined the cervical skeleton of the Moz−/− mice. The neural arches of the cervical vertebrae were fused, and those of the axis and C3 were thickened in Moz−/− mice (Figs. 9H, I). Notably, the morphological feature of C3 neural arch has changed to that of axis (Figs. 9H, I, asterisks). In addition, the atlas was fused to the exoccipitals in the Moz−/− mice (Figs. 9J–M). In the posterior region, the Moz−/− mice had a kinky tail, although we failed to find an abnormality of posterior cartilage formation in the Moz−/− mice (Supplementary Figs. 7E, F). These results suggest that the MOZ HAT complex plays an essential role for the proper skeletal patterning in mice.

MOZ HAT complex was required for the transcriptional regulation of anterior and posterior Hox genes in mice

Moz−/− mice exhibited the similar phenotype in cervical cartilage to that in Hox4 deficient mice (Horan et al., 1995). We then examined whether the MOZ HAT complex was required for the maintenance of expression of *Hox* genes. The expression of *Hoxa3* and *Hoxa4* were mildly decreased at the rhombomere and neural tube in Moz−/− mice (Figs. 10A, B, arrowheads). On the other hand, their expressions were severely reduced at the somite (Figs. 10A, B, arrows). Consistent with the observation of the medaka *brpf1* mutant, in Moz−/− mice, the expressions of *Hoxa3* and *Hoxa4* were also decreased at the third and fourth pharyngeal arch, respectively (Figs. 10A, B, arrows in lower panels). Although the decrease of *Hoxa3* expression was observed, it was less severe than that of *Hoxa4* expression at the pharyngeal arch. Furthermore, we examined the expression of posterior *Hox* genes; *Hoxd10* and *Hoxd11*. In Moz−/− mice, the expressions of *Hoxd10* and *Hoxd11* were also reduced at the somite (Figs. 10C, D, arrows). These results suggest that, in mice, the MOZ HAT complex were also required for the maintenance of the expression of anterior and posterior *Hox* genes.

Discussion

In this study, we characterized the *bis* mutant in medaka, which exhibits defects in the development of its craniofacial and caudal skeletons. The expression of *Hox* genes was decreased during development of the *bis* mutant, compared with that of the wild type. Genetic analysis and the rescue experiment demonstrated that the loss of Brpf1 function was the cause of the *bis* phenotypes. Brpf1 is a partner of the MOZ HAT complex, which is essential for the maintenance of the expression of *Hox* genes, suggesting that the segmental identities along the A–P axis, which are governed by *Hox* genes, are disrupted in the *bis* mutant. Thus, we conclude that Brpf1 maintains the expression of *Hox* genes by regulating the modification of chromatin.

Brpf1 behaves as a part of the MOZ HAT complex functionally in skeletal development

Brpf1 contains multiple domains with the affinity for the modulated histone tail, suggesting that Brpf1 regulates transcription via modulating the chromatin structure. Previous studies showed that Brpf1 is a member of the MOZ HAT complex (Doyon et al., 2006; Yang and Ullah, 2007). Targeted inactivation of Moz in mice resulted in reduced hematopoiesis and decreased expression of *Hoxa9* gene in fetal liver (Katsumoto et al., 2006; Thomas et al., 2006). In addition, spleen formation was disrupted in the Moz−/− mice. We also observed that spleen formation was disrupted in the *bis* mutant (data not shown). ENU-induced mutation of the *moz* gene in zebrafish causes the homeotic transformation of the craniofacial cartilage and the decreased expression of *Hox* genes in the pharyngeal arches (Crump et al., 2006; Miller et al., 2004). Recently, phenotypes of the ENU-induced zebrafish mutant *brpf1* were shown to be similar to those of the zebrafish *moz* mutant, and the expression of *Hox* genes in the pharyngeal arches was decreased in the zebrafish *brpf1* mutant (Laue et al., 2008). Consistent with these previous reports, the *bis* mutant exhibited the anterior transformation of craniofacial cartilage and the deceased expression of *Hox* genes. In this study, we performed the *brpf1* morpholino anti-sense oligo experiment; however we failed in the phenocopy of *bis* mutant (data not shown), because the developmental stage of the establishment of pharyngeal arch

Please cite this article as: Hibiya, K., et al., Brpf1, a subunit of the MOZ histone acetyl transferase complex, maintains expression of anterior and posterior *Hox* genes for prope... Dev. Biol. (2009), doi:10.1016/j.ydbio.2009.02.021

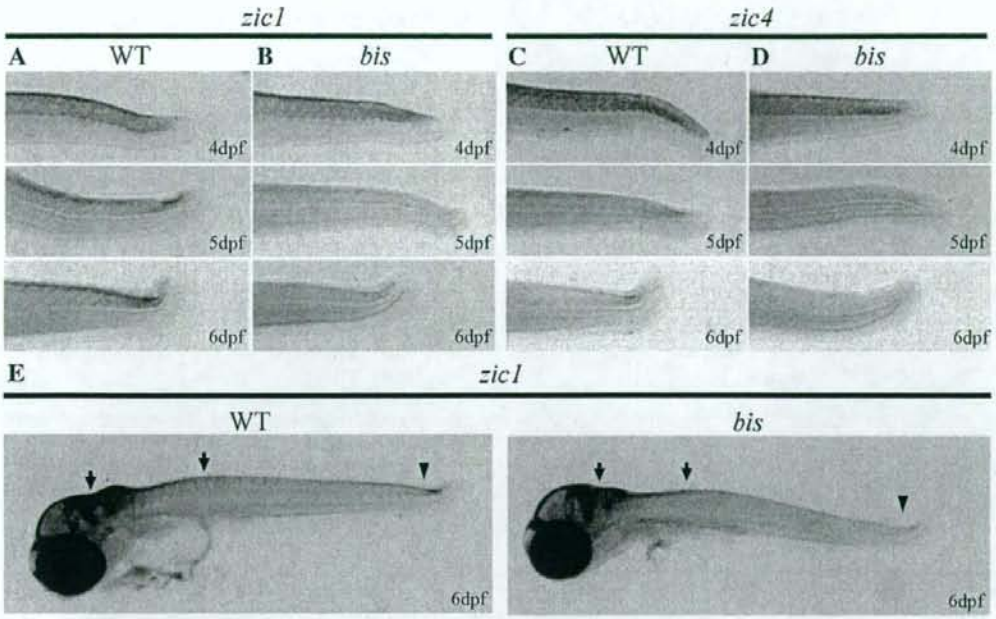

Fig. 8. The *bis* mutant exhibits decreased expression of *Zic* genes. Lateral views are given in all photos. (A, B) Expression of *zic1* in the posterior region in the wild type and the *bis* mutant. Although the expression of *zic1* is normally expressed in the *bis* mutant at 4 dpf, the expression gradually decreases at 5 and 6 dpf. (C, D) Expression of *zic4* in the posterior region in the wild type and the *bis* mutant. The expression of *zic4* is normal in the *bis* mutant at 4 dpf, whereas it gradually decreases at 5 and 6 dpf. (E) Lateral view of the expression of *zic1* in the wild type and *bis* larvae. Although the expression of *zic1*was decreased at the caudal tissue (arrowhead), it was not affected in the anterior neural tube and hindbrain (arrow).

identity in medaka was later than that in zebrafish. Alternatively, we demonstrated that re-introduction of the normal *brpf1* gene into the *bis* mutant could rescue the *bis* phenotype, and inhibition of HDAC activity partially rescued the phenotype of *bis* mutant (Supplementary result, Supplementary Fig. 6 and Supplementary Table 1); although, the efficiency of TSA treatment in the *bis* mutant was significantly lower than that of the zebrafish *moz* and *brpf1* mutants, probably due to the different sensitivity to TSA between two species. Thus, we suggest that Brpf1 behaves as a part of MOZ complex functionally in skeletal development.

The decreased expression of Hox genes in the pharyngeal arches causes homeotic transformation in the bis mutant

Our study demonstrates that Brpf1 is required for the proper patterning of the craniofacial cartilage, which is derived from neural crest cells that migrate from the hindbrain. Hox signaling has been implicated in the establishment of segmental identities of cranial neural crest cells. Hox2-group genes determine the identity of the second arch. A mutation in the *Hoxa2* gene in mice or knock down of *hoxa2b* and *hoxb2a* genes in zebrafish leads to a homeotic transformation of the second arch to the first arch identity (Gendron-Maguire et al., 1993; Hunter and Prince, 2002). The *bis* mutant exhibited the partial transformation of the second arch to the first identity, which is consistent with the deceased expression of the *hoxb2a* gene. Although zebrafish *moz* and *brpf1* mutants exhibited a complete transformation of the second arch identity to the first arch identity, the skeletal transformation of the second arch element was not significant in the *bis* mutant. This phenotypic difference between zebrafish and medaka may be due to the difference in the Hox cluster evolution. For example, although the expression of *hoxa2a* was maintained in the second pharyngeal arch in the *bis* mutant, *hoxa2a* does not exist in zebrafish (Hoegg et al., 2007; Kurosawa et al., 2006), suggesting that a Hox paralogue group, *hoxa2a*, has a functional redundancy in determining the A–P axis identity in the *bis* mutant. Thus, in the disruption of Brpf1 function, the other redundant mechanism may act in the maintenance of the expression of *hoxa2a*.

The *bis* mutant displayed decreased expression of *Hox3* genes and ectopic expression of *gsc* in the third pharyngeal arch, implying that the segmental identity of the third pharyngeal arch had changed to that of the second pharyngeal arch in the *bis* mutant. A loss of the thymus in the Hox3 group knock-out mice is consistent with that in the *bis* mutant (Manley and Capecchi, 1995, 1998). Furthermore, the fusion of the first vertebra to the head skeleton in the *bis* mutant probably corresponds to the similar phenotype in the Hox3 group knock-out mice (Condie and Capecchi, 1994; Manley and Capecchi, 1997). Although skeletal phenotypes of knock-out mice of the Hox3 paralogue group did not display an apparent transformation of the third arch-derived structure, the decreased expression of *Hox3* genes in the *valentino* mutant of zebrafish and the *kreisler* mutant of mice causes ectopic cartilage formation in the third pharyngeal arch, whose characteristic features resemble the hyoid derived from the second arch (Frohman et al., 1993; Manzanares et al., 1999; Moens et al., 1998; Prince et al., 1998). Thus, the decreased expression of *Hox3* genes might cause the homeotic transformation of the third arch identity into the second arch identity in the *bis* mutant.

The abnormality in D–V axis formation in the caudal fin occurs due to decreased expression of Zic genes in the bis mutant

The *bis* mutant exhibited abnormalities in its posterior skeletal patterning. Although these phenotypes were not described in *moz*

Please cite this article as: Hibiya, K., et al., Brpf1, a subunit of the MOZ histone acetyl transferase complex, maintains expression of anterior and posterior *Hox* genes for prope..., Dev. Biol. (2009), doi:10.1016/j.ydbio.2009.02.021

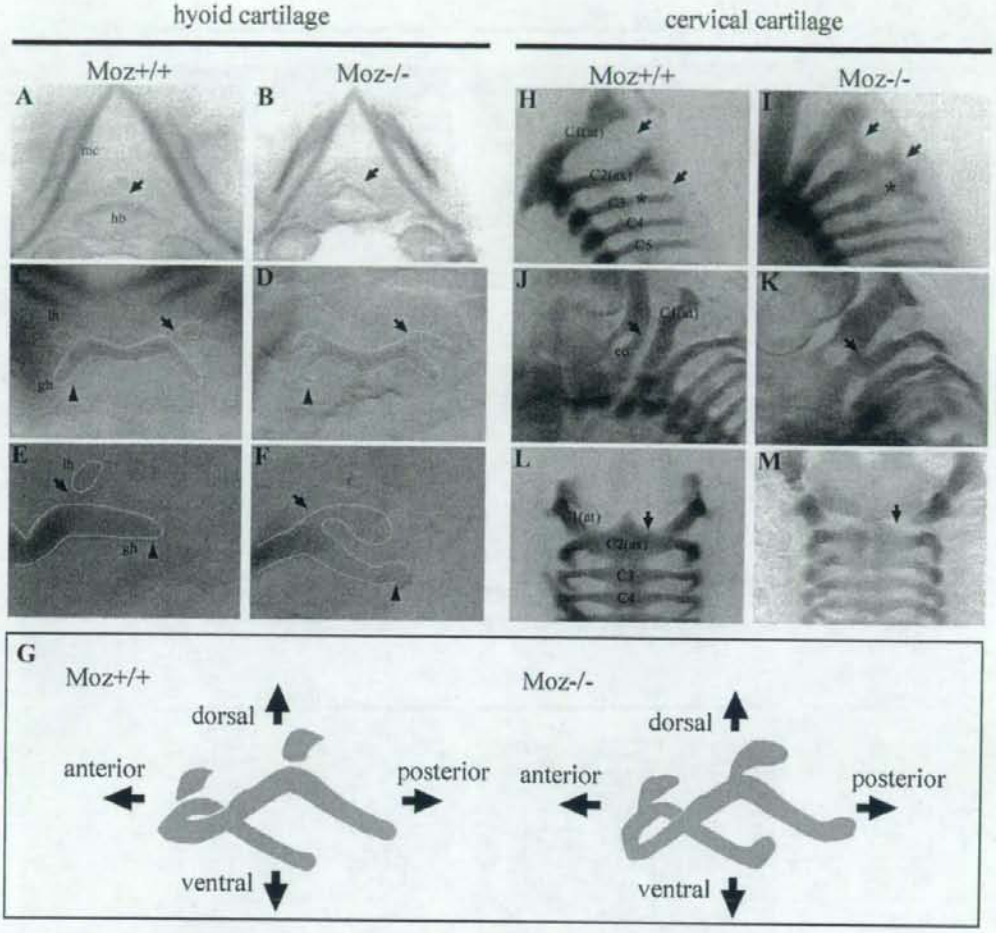

Fig. 9. Moz−/− mice exhibit abnormal patterning in hyoid and cervical cartilages (A–F). The hyoid cartilage was stained with Alcian blue. (A, B) Ventral views of the hyoid cartilage. The hyoid body is seen (arrows), which in the Moz−/− mice has morphological similarity to Meckel's cartilage. (C, D) Anterior views of the hyoid cartilage. The lesser horn of the hyoid (arrows) has fused to the hyoid body in the Moz−/− mice but not in the wild type; and an accessory process is notable on the greater horn of the hyoid in the mutant (arrowhead) but is absent in the wild-type (arrow indicating its absence). (E, F) Dorsal–lateral view of the greater horn of the hyoid, showing the same phenotypes as seen in the anterior view. (G) A schematic of the hyoid cartilage in the wild type +/+ and Moz−/− mice. (H–M) Cervical cartilages were stained with Alcian blue. (H, I) Lateral views of the cervical cartilage. The neural arches of atlas, axis, and C3 (arrows) are fused in the Moz−/− mice. The morphological feature of the neural arch of C3 (asterisks) has changed to that of the axis. (J, K) Dorsal–lateral views of the cervical cartilage. The atlas (arrows) has fused to the exoccipital in the Moz−/− mice. (L, M) Dorsal views of the cervical cartilage. The ventral part of the atlas (arrows) has been deleted in the Moz−/− mice. mc, Meckel's cartilage; hb, hyoid body; lh, lesser horn of hyoid; gh, greater horn of hyoid; C1–C5, cervical vertebra 1 to 5; at, atlas; ax, axis.

and *brpf1* mutants in zebrafish, the expression of *brpf1* itself exists in the posterior trunk region in zebrafish (ZFIN: MGC55530). The *bis* mutant exhibited the D–V axis disruption in its caudal fin. Our study revealed that the expression of *zic1* and *zic4* genes in the posterior trunk region was severely decreased in the *bis* mutant, suggesting that the disruption of the D–V axis was due to the decreased expression of these genes.

The *bis* mutant also exhibited decreased expression of *Hox* genes in the posterior trunk region. It should be noted that their expression decreased earlier than that of *Zic* genes in the posterior region (Figs. 6 and 8). Furthermore, in the *Da* mutant, *Hox* genes were normally expressed in the posterior region. Although no other previous reports have described the relationship between *Hox* genes and *Zic* genes *in vivo*, the Chip-on-Chip assay for Hoxa13 showed that the Hoxa13 protein binds to the *zic1* and *zic4* promoter sequence (Rinn et al., 2008). Therefore, our findings suggest that Brpf1 regulates the expression of *Zic* genes via the regulation of *Hox* genes.

The decreased expression of Hox genes causes the abnormal patterning of caudal vertebrae in the bis mutant

The *bis* mutant exhibited similar phenotypes as the *Da* mutant in its caudal fin. On the other hand, the phenotypes of caudal vertebra and hypural were different between the 2 mutants. This result indicates that this abnormality is caused independently by the decreased expression of *Zic* genes. The targeted disruption of *Hox13* genes results in the anterior transformation or an increased number of caudal vertebrae (Dolle et al., 1993; Economides et al., 2003;

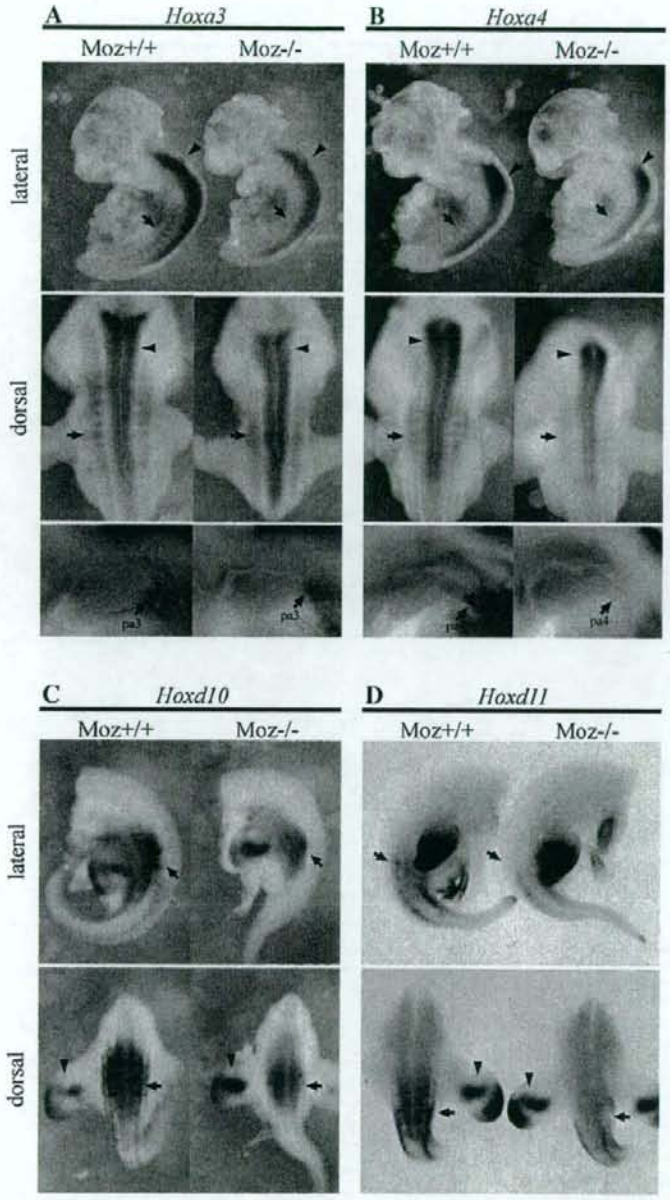

Fig. 10. Moz−/− mice exhibited the decrease of the expression of anterior and posterior *Hox* genes. Whole-mount *in situ* hybridization was performed at E11.5 in the wild type and Moz−/− mice. (A) Expressions of *Hoxa3* in the wild type and Moz−/− mice. Expressions of *Hoxa3* were mildly decreased in the rhombomere and neural tube in Moz−/− mice (arrowheads in upper and middle panels). On the other hand, their expressions were decreased at the somite in Moz−/− mice (arrows in upper and middle panels). Expressions of *Hoxa3* were mildly decreased at the third pharyngeal arch in Moz−/− mice (arrows in lower panels). (B) Expressions of *Hoxa4* in the wild type and Moz−/− mice. A similar decrease was observed in Moz−/− mice (arrows and arrowheads in upper and middle panels). Note that the expressions of *Hoxa4* at the pharyngeal arches were severely decreased in Moz−/− mice (arrows in lower panels). (C) Expressions of *Hoxd10* in the wild type and Moz−/− mice. The expression of the *Hoxd10* was severely decreased in the somite and neural tube (arrows). However the expression of *Hoxd10* in the hind limb was not decreased (arrowheads). (D) Expressions of *Hoxd11* in the wild type and Moz−/− mice. Expressions of *Hoxd11* were also decreased at the somite and neural tube in Moz−/− mice (arrow). Expressions of *Hoxd11* were not affected at the hind limb (arrowhead). pa3; third pharyngeal arch, pa4; fourth pharyngeal arch.

Godwin and Capecchi, 1998). Although an apparent transformation of vertebral morphology was not observed in the *bis* mutant, the hypurals of the caudal vertebrae were reduced in size or disappeared in the *bis* mutant. This phenotype might be caused by the partial transformation of caudal vertebrae into the morphology of anterior ones.

Please cite this article as: Hibiya, K., et al., Brpf1, a subunit of the MOZ histone acetyl transferase complex, maintains expression of anterior and posterior *Hox* genes for prope.... Dev. Biol. (2009), doi:10.1016/j.ydbio.2009.02.021

Gene-specific regulation by Brpf1 in the anterior and posterior regions

In this study, we demonstrated that Brpf1 regulates the expression of *Hox* genes in the anterior and posterior regions of the developing body but not that of those in the central region. Previous studies on the function of TrxG mainly were performed on *mll* knock-out mice and focused on the gene-specific regulation of *Hox* genes. In *mll* knock-out mice, the expression of *hoxa7*, *hoxd4*, and *hoxc8* was decreased at the central region of the developing embryo (Glaser et al., 2006; Terranova et al., 2006; Yu et al., 1998, 1995). On the other hand, the *bis* mutant exhibited decreased expression of *Hox* genes in the anterior and posterior regions. It should be noted that the expression of *Hox* genes located at the center of the Hox cluster and expressed in the central region of the developing embryo was not affected or only mildly decreased in the *bis* mutant (Supplementary Fig. 5), implying the gene-specific regulation of Brpf1 in the maintenance of the expression of the *Hox* genes. In A–P axis formation, in addition to *Hox* genes, FGF and RA signals are also involved in the initial establishment of A–P axis formation (Bel-Vialar et al., 2002; Diez del Corral and Storey, 2004). FGF preferentially functions in the anterior and posterior axial formation, whereas RA preferentially functions in the central axial formation. The regions where the expression of *Hox* genes was decreased in the *bis* mutant have a strong relation to the FGF organizing area, suggesting that MOZ HAT complex may collaborate with FGF signaling in the regulation of *Hox* gene expression. In addition, although the expression of *Hox* genes was decreased in various regions of the developing body of the *bis* mutant, the expression of some *Hox* genes was only mildly decreased at certain restricted regions, e.g., hindbrain, posterior pharyngeal arch. These findings suggest that a different requirement for Brpf1 exists at the different regions or that some other factors function redundantly at these regions. To estimate the functional redundancy of Brpf1, we examined the expression of all Brpf families, which include *brpf1*, *brpf2*, and *brpf3*, and found that these genes were expressed in similar regions (data not shown), indicating that *brpf2* and *brpf3* have no functional redundancy in maintaining the Hox expression. In this study, the detailed mechanisms which underlie the maintenance of *Hox* genes have not been clarified. A further study is required to elucidate how the expression of each *Hox* gene in various tissues is differently regulated by the chromatin regulation.

A common role of the MOZ HAT complex in skeletal development via regulating the expression of Hox genes

In this study, we also demonstrated the abnormality of the skeletal patterning in the Moz−/− mice. The shape of the hyoid cartilage was changed in the Moz−/− mice. In the ventral view, the shape of hyoid body was similar to that of Meckel's cartilage. In addition, the accessory process on the greater horn of the hyoid in the Moz−/− mice was similar to the phenotype of *kreisler* mutant mice and zebrafish *valentine* mutant, in which the reduced expression of *Hox3* genes is observed, and the lesser horn of the hyoid is ectopically formed on the greater horn of the hyoid (Frohman et al., 1993; Kimmel et al., 2001; Manzanares et al., 1999; Prince et al., 1998). Consistent with these reports, Moz−/− mice exhibit the reduction of *Hoxa3* transcript at the third pharyngeal arch. In the cervical region, the axis was fused to the exoccipital in the Moz−/− mice. A similar phenotype was demonstrated in the Hox 3 paralogue group knock-out mice (Condie and Capecchi, 1994; Manley and Capecchi, 1997). Furthermore, the neural arch of the C3 had a morphological similarity to that of the axis, and the fused neural arches in cervical vertebrae were similar to those of the *Hoxa4* and *Hoxb4* double knock-out mice (Horan et al., 1995). Consistently, *Hoxa4* transcripts were decreased at the somite in Moz−/− mice, suggesting that the abnormality of cervical vertebrae was caused by A–P axis disruption. Furthermore, in the posterior region, the Moz−/− mice exhibited a decrease of *Hoxd10* and *Hoxd11* expressions. However, we failed to find abnormalities of cartilage formation in the Moz−/− mice at the position of the hind limb (data not shown). It may be possible that finding the abnormality of the Moz−/− mice was difficult, because the posterior skeleton has not fully formed at E14.5. Thus, these results suggest that the abnormal skeletal phenotypes of the Moz−/− mice were caused by the decreased expressions of *Hox* genes, and the common mechanism using MOZ HAT complex exists in the skeletal patterning in vertebrate development.

Acknowledgments

We thank Dr. N. Manley, Dr. M. Araki and Dr. X.J Yang for their kindly gifts of mouse *Hoxa3*, *Hoxa4* and Flag-Moz and HA-Brpf1 plasmid, respectively. We thank Dr. K. Naruse for a gift of the BAC vector, Dr. K. Maruyama for a gift of the α-*globin*-GFP transgenic medaka, Dr. K. Inohaya and Dr. A. Kawakami for many helpful discussions, and finally Dr. I. Kii for reading of manuscript. We also would like to express sincere appreciation to our colleagues for their support during the screening of medaka mutants. We also thank NBRP Medaka for providing a hatching enzyme. This work was supported by grants-in-aid from the Ministry of Education, Culture, Sports, Science, and Technology of Japan.

Appendix A. Supplementary data

Supplementary data associated with this article can be found, in the online version, at doi:10.1016/j.ydbio.2009.02.021.

References

Akasaka, T., Kanno, M., Balling, R., Mieza, M.A., Taniguchi, M., Koseki, H., 1996. A role for mel-18, a Polycomb group-related vertebrate gene, during the anteroposterior specification of the axial skeleton. Development 122, 1513–1522.

Akasaka, T., van Lohuizen, M., van der Lugt, N., Mizutani-Koseki, Y., Kanno, M., Taniguchi, M., Vidal, M., Alkema, M., Berns, A., Koseki, H., 2001. Mice doubly deficient for the polycomb group genes Mel18 and Bmi1 reveal synergy and requirement for maintenance but not initiation of *Hox* gene expression. Development 128, 1587–1597.

Beddington, R.S., Robertson, E.J., 1999. Axis development and early asymmetry in mammals. Cell 96, 195–209.

Bel-Vialar, S., Itasaki, N., Krumlauf, R., 2002. Initiating *Hox* gene expression: in the early chick neural tube differential sensitivity to FGF and RA signaling subdivides the *HoxB* genes in two distinct groups. Development 129, 5103–5115.

Condie, B.G., Capecchi, M.R., 1994. Mice with targeted disruptions in the paralogous genes hoxa-3 and hoxd-3 reveal synergistic interactions. Nature 370, 304–307.

Core, N., Bel, S., Gaunt, S.J., Aurrand-Lions, M., Pearce, J., Fisher, A., Djabali, M., 1997. Altered cellular proliferation and mesoderm patterning in polycomb-M33-deficient mice. Development 124, 721–729.

Crump, J.G., Swartz, M.E., Eberhart, J.K., Kimmel, C.B., 2006. Moz-dependent Hox expression controls segment-specific fate maps of skeletal precursors in the face. Development 133, 2661–2669.

del Mar Lorente, M., Marcos-Gutierrez, C., Perez, C., Schoorlemmer, J., Ramirez, A., Magin, T., Vidal, M., 2000. Loss- and gain-of-function mutations show a polycomb group function for Ring1A in mice. Development 127, 5093–5100.

Deschamps, J., van den Akker, E., Forlani, S., De Graaff, W., Oosterveen, T., Roelen, B., Roelfsema, J., 1999. Initiation, establishment and maintenance of *Hox* gene expression patterns in the mouse. Int. J. Dev. Biol. 43, 635–650.

Deschamps, J., van Nes, J., 2005. Developmental regulation of the *Hox* genes during axial morphogenesis in the mouse. Development 132, 2931–2942.

Dhalluin, C., Carlson, J.E., Zeng, L., He, C., Aggarwal, A.K., Zhou, M.M., 1999. Structure and ligand of a histone acetyltransferase bromodomain. Nature 399, 491–496.

Diez del Corral, R., Storey, K.G., 2004. Opposing FGF and retinoid pathways: a signalling switch that controls differentiation and patterning onset in the extending vertebrate body axis. Bioessays 26, 857–869.

Dolle, P., Dierich, A., LeMeur, M., Schimmang, T., Schuhbaur, B., Chambon, P., Duboule, D., 1993. Disruption of the *Hoxd-13* gene induces localized heterochrony leading to mice with neotenic limbs. Cell 75, 431–441.

Doyon, Y., Cayrou, C., Ullah, M., Landry, A.J., Cote, V., Selleck, W., Lane, W.S., Tan, S., Yang, X.J., Cote, J., 2006. ING tumor suppressor proteins are critical regulators of chromatin acetylation required for genome expression and perpetuation. Mol. Cell 21, 51–64.

Economides, K.D., Zeltser, L., Capecchi, M.R., 2003. Hoxb13 mutations cause overgrowth of caudal spinal cord and tail vertebrae. Dev. Biol. 256, 317–330.

Favier, B., Dolle, P., 1997. Developmental functions of mammalian *Hox* genes. Mol. Hum. Reprod. 3, 115–131.

Frohman, M.A., Martin, G.R., Cordes, S.P., Halamek, L.P., Barsh, G.S., 1993. Altered rhombomere-specific gene expression and hyoid bone differentiation in the mouse segmentation mutant, kreisler (kr). Development 117, 925–936.

Gendron-Maguire, M., Mallo, M., Zhang, M., Gridley, T., 1993. Hoxa-2 mutant mice exhibit homeotic transformation of skeletal elements derived from cranial neural crest. Cell 75, 1317–1331.

Glaser, S., Schaft, J., Lubitz, S., Vintersten, K., van der Hoeven, F., Tufteland, K.R., Aasland, R., Anastassiadis, K., Ang, S.L., Stewart, A.F., 2006. Multiple epigenetic maintenance factors implicated by the loss of Mll2 in mouse development. Development 133, 1423–1432.

Godwin, A.R., Capecchi, M.R., 1998. Hoxc13 mutant mice lack external hair. Genes Dev. 12, 11–20.

Hadzhiev, Y., Lele, Z., Schindler, S., Wilson, S.W., Ahlberg, P., Strahle, U., Muller, F., 2007. Hedgehog signaling patterns the outgrowth of unpaired skeletal appendages in zebrafish. BMC Dev. Biol. 7, 75.

Hoegg, S., Boore, J.L., Kuehl, J.V., Meyer, A., 2007. Comparative phylogenomic analyses of teleost fish *Hox* gene clusters: lessons from the cichlid fish *Astatotilapia burtoni*. BMC Genomics 8, 317.

Horan, G.S., Ramirez-Solis, R., Featherstone, M.S., Wolgemuth, D.J., Bradley, A., Behringer, R.R., 1995. Compound mutants for the paralogous hoxa-4, hoxb-4, and hoxd-4 genes show more complete homeotic transformations and a dose-dependent increase in the number of vertebrae transformed. Genes Dev. 9, 1667–1677.

Hunter, M.P., Prince, V.E., 2002. Zebrafish hox paralogue group 2 genes function redundantly as selector genes to pattern the second pharyngeal arch. Dev. Biol. 247, 367–389.

Inohaya, K., Yasumasu, S., Ishimaru, M., Ohyama, A., Iuchi, I., Yamagami, K., 1995. Temporal and spatial patterns of gene expression for the hatching enzyme in the teleost embryo, *Oryzias latipes*. Dev. Biol. 171, 374–385.

Inohaya, K., Yasumasu, S., Yasumasu, I., Iuchi, I., Yamagami, K., 1999. Analysis of the origin and development of hatching gland cells by transplantation of the embryonic shield in the fish, *Oryzias latipes*. Dev. Growth Differ. 41, 557–566.

Iwamatsu, T., 2004. Stages of normal development in the medaka *Oryzias latipes*. Mech. Dev. 121, 605–618.

Izpisua-Belmonte, J.C., Falkenstein, H., Dolle, P., Renucci, A., Duboule, D., 1991. Murine genes related to the *Drosophila* AbdB homeotic genes are sequentially expressed during development of the posterior part of the body. EMBO J. 10, 2279–2289.

Katsumoto, T., Aikawa, Y., Iwama, A., Ueda, S., Ichikawa, H., Ochiya, T., Kitabayashi, I., 2006. MOZ is essential for maintenance of hematopoietic stem cells. Genes Dev. 20, 1321–1330.

Kawazoe, Y., Sekimoto, T., Araki, M., Takagi, K., Araki, K., Yamamura, K., 2002. Region-specific gastrointestinal Hox code during murine embryonal gut development. Dev. Growth Differ. 44, 77–84.

Kimmel, C.B., Miller, C.T., Moens, C.B., 2001. Specification and morphogenesis of the zebrafish larval head skeleton. Dev. Biol. 233, 239–257.

Kimura, T., Jindo, T., Narita, T., Naruse, K., Kobayashi, D., Shin-i, T., Kitagawa, T., Sakaguchi, T., Mitani, H., Shima, A., et al., 2004. Large-scale isolation of ESTs, from medaka embryos and its application to medaka developmental genetics. Mech. Dev. 121, 915–932.

Kmita, M., Duboule, D., 2003. Organizing axes in time and space; 25 years of colinear tinkering. Science 301, 331–333.

Kondo, T., Duboule, D., 1999. Breaking colinearity in the mouse HoxD complex. Cell 97, 407–417.

Kuratani, S., 2005. Developmental studies of the lamprey and hierarchical evolutionary steps towards the acquisition of the jaw. J. Anat. 207, 489–499.

Kurosawa, G., Takamatsu, N., Takahashi, M., Sumitomo, M., Sanaka, E., Yamada, K., Nishii, K., Matsuda, M., Asakawa, S., Ishiguro, H., et al., 2006. Organization and structure of *hox* gene loci in medaka genome and comparison with those of pufferfish and zebrafish genomes. Gene 370, 75–82.

Laue, K., Daujat, S., Crump, J.G., Plaster, N., Roehl, H.H., Kimmel, C.B., Schneider, R., Hammerschmidt, M., 2008. The multidomain protein Brpf1 binds histones and is required for *Hox* gene expression and segmental identity. Development 135, 1935–1946.

Le Douarin, N.M., Jotereau, F.V., 1975. Tracing of cells of the avian thymus through embryonic life in interspecific chimeras. J. Exp. Med. 142, 17–40.

Lewis, E.B., 1978. A gene complex controlling segmentation in *Drosophila*. Nature 276, 565–570.

Lumsden, A., Sprawson, N., Graham, A., 1991. Segmental origin and migration of neural crest cells in the hindbrain region of the chick embryo. Development 113, 1281–1291.

Manley, N.R., Capecchi, M.R., 1995. The role of Hoxa-3 in mouse thymus and thyroid development. Development 121, 1989–2003.

Manley, N.R., Capecchi, M.R., 1997. Hox group 3 paralogous genes act synergistically in the formation of somitic and neural crest-derived structures. Dev. Biol. 192, 274–288.

Manley, N.R., Capecchi, M.R., 1998. Hox group 3 paralogs regulate the development and migration of the thymus, thyroid, and parathyroid glands. Dev. Biol. 195, 1–15.

Manley, N.R., Selleri, L., Brendolan, A., Gordon, J., Cleary, M.L., 2004. Abnormalities of caudal pharyngeal pouch development in Pbx1 knockout mice mimic loss of Hox3 paralogs. Dev. Biol. 276, 301–312.

Manzanares, M., Trainor, P.A., Nonchev, S., Ariza-McNaughton, L., Brodie, J., Gould, A., Marshall, H., Morrison, A., Kwan, C.T., Sham, M.H., et al., 1999. The role of kreisler in segmentation during hindbrain development. Dev. Biol. 211, 220–237.

Miller, C.T., Maves, L., Kimmel, C.B., 2004. moz regulates Hox expression and pharyngeal segmental identity in zebrafish. Development 131, 2443–2461.

Moens, C.B., Cordes, S.P., Giorgianni, M.W., Barsh, G.S., Kimmel, C.B., 1998. Equivalence in the genetic control of hindbrain segmentation in fish and mouse. Development 125, 381–391.

Mullins, M.C., Hammerschmidt, M., Haffter, P., Nusslein-Volhard, C., 1994. Large-scale mutagenesis in the zebrafish: in search of genes controlling development in a vertebrate. Curr. Biol. 4, 189–202.

Naruse, K., Fukamachi, S., Mitani, H., Kondo, M., Matsuoka, T., Kondo, S., Hanamura, N., Morita, Y., Hasegawa, K., Nishigaki, R., et al., 2000. A detailed linkage map of medaka, *Oryzias latipes*: comparative genomics and genome evolution. Genetics 154, 1773–1784.

Noden, D.M., 1978. The control of avian cephalic neural crest cytodifferentiation. I. Skeletal and connective tissues. Dev. Biol. 67, 296–312.

Noden, D.M., 1988. Interactions and fates of avian craniofacial mesenchyme. Development 103, 121–140 Suppl.

Ohtsuka, M., Kikuchi, N., Yokoi, H., Kinoshita, M., Wakamatsu, Y., Ozato, K., Takeda, H., Inoko, H., Kimura, M., 2004. Possible roles of zic1 and zic4, identified within the medaka Double anal fin (Da) locus, in dorsoventral patterning of the trunk–tail region (related to phenotypes of the Da mutant). Mech. Dev. 121, 873–882.

Papp, B., Muller, J., 2006. Histone trimethylation and the maintenance of transcriptional ON and OFF states by trxG and PcG proteins. Genes Dev. 20, 2041–2054.

Pena, P.V., Davrazou, F., Shi, X., Walter, K.L., Verkhusha, V.V., Gozani, O., Zhao, R., Kutateladze, T.G., 2006. Molecular mechanism of histone H3K4me3 recognition by plant homeodomain of ING2. Nature 442, 100–103.

Piotrowski, T., Nusslein-Volhard, C., 2000. The endoderm plays an important role in patterning the segmented pharyngeal region in zebrafish (*Danio rerio*). Dev. Biol. 225, 339–356.

Prince, V.E., Moens, C.B., Kimmel, C.B., Ho, R.K., 1998. Zebrafish *hox* genes: expression in the hindbrain region of wild-type and mutants of the segmentation gene, *valentino*. Development 125, 393–406.

Rancourt, D.E., Tsuzuki, T., Capecchi, M.R., 1995. Genetic interaction between hoxb-5 and hoxb-6 is revealed by nonallelic noncomplementation. Genes Dev. 9, 108–122.

Renucci, A., Zappavigna, V., Zakany, J., Izpisua-Belmonte, J.C., Burki, K., Duboule, D., 1992. Comparison of mouse and human HOX-4 complexes defines conserved sequences involved in the regulation of Hox-4.4. EMBO J. 11, 1459–1468.

Rinn, J.L., Wang, J.K., Allen, N., Brugmann, S.A., Mikels, A.J., Liu, H., Ridky, T.W., Stadler, H.S., Nusse, R., Helms, J.A., et al., 2008. A dermal HOX transcriptional program regulates site-specific epidermal fate. Genes Dev. 22, 303–307.

Rivera-Perez, J.A., Mallo, M., Gendron-Maguire, M., Gridley, T., Behringer, R.R., 1995. Goosecoid is not an essential component of the mouse gastrula organizer but is required for craniofacial and rib development. Development 121, 3005–3012.

Rokudai, S., Aikawa, Y., Tagata, Y., Tsuchida, N., Taya, Y., Kitabayashi, I., 2009. Monocytic leukemia zinc finger (MOZ) interacts with p53 to induce p21 expression and cell-cycle arrest. J. Biol. Chem. 284, 237–244.

Sakaguchi, S., Nakatani, Y., Takamatsu, N., Hori, H., Kawakami, A., Inohaya, K., Kudo, A., 2006. Medaka unextended-fin mutants suggest a role for Hoxb8a in cell migration and osteoblast differentiation during appendage formation. Dev. Biol. 293, 426–438.

Santagati, F., Minoux, M., Ren, S.Y., Rijli, F.M., 2005. Temporal requirement of Hoxa2 in cranial neural crest skeletal morphogenesis. Development 132, 4927–4936.

Solnica-Krezel, L., Schier, A.F., Driever, W., 1994. Efficient recovery of ENU-induced mutations from the zebrafish germline. Genetics 136, 1401–1420.

Soshnikova, N., Duboule, D., 2008. Epigenetic regulation of *Hox* gene activation: the waltz of methyls. Bioessays 30, 199–202.

Suzuki, M., Mizutani-Koseki, Y., Fujimura, Y., Miyagishima, H., Kaneko, T., Takada, Y., Akasaka, T., Tanzawa, H., Takihara, Y., Nakano, M., et al., 2002. Involvement of the Polycomb-group gene Ring1B in the specification of the anterior–posterior axis in mice. Development 129, 4171–4183.

Takihara, Y., Tomotsune, D., Shirai, M., Katoh-Fukui, Y., Nishii, K., Motaleb, M.A., Nomura, M., Tsuchiya, R., Fujita, Y., Shibata, Y., et al., 1997. Targeted disruption of the mouse homologue of the *Drosophila* polyhomeotic gene leads to altered anteroposterior patterning and neural crest defects. Development 124, 3673–3682.

Tanaka, K., Ohisa, S., Orihara, N., Sakaguchi, S., Horie, K., Hibiya, K., Konno, S., Miyake, A., Setiamarga, D., Takeda, H., et al., 2004. Characterization of mutations affecting embryonic hematopoiesis in the medaka, *Oryzias latipes*. Mech. Dev. 121, 739–746.

Taverna, S.D., Ilin, S., Rogers, R.S., Tanny, J.C., Lavender, H., Li, H., Baker, L., Boyle, J., Blair, L.P., Chait, B.T., et al., 2006. Yng1 PHD finger binding to H3 trimethylated at K4 promotes NuA3 HAT activity at K14 of H3 and transcription at a subset of targeted ORFs. Mol. Cell 24, 785–796.

Terranova, R., Agherbi, H., Boned, A., Meresse, S., Djabali, M., 2006. Histone and DNA methylation defects at *Hox* genes in mice expressing a SET domain-truncated form of Mll. Proc. Natl. Acad. Sci. U. S. A. 103, 6629–6634.

Thermes, V., Grabher, C., Ristoratore, F., Bourrat, F., Choulika, A., Wittbrodt, J., Joly, J.S., 2002. I-SceI meganuclease mediates highly efficient transgenesis in fish. Mech. Dev. 118, 91–98.

Thomas, T., Corcoran, L.M., Gugasyan, R., Dixon, M.P., Brodnicki, T., Nutt, S.L., Metcalf, D., Voss, A.K., 2006. Monocytic leukemia zinc finger protein is essential for the development of long-term reconstituting hematopoietic stem cells. Genes Dev. 20, 1175–1186.

Tucker, A.S., Watson, R.P., Lettice, L.A., Yamada, G., Hill, R.E., 2004. Bapx1 regulates patterning in the middle ear: altered regulatory role in the transition from the proximal jaw during vertebrate evolution. Development 131, 1235–1245.

Turlure, F., Maertens, G., Rahman, S., Cherepanov, P., Engelman, A., 2006. A tripartite DNA-binding element, comprised of the nuclear localization signal and two AT-hook motifs, mediates the association of LEDGF/p75 with chromatin in vivo. Nucleic Acids Res. 34, 1653–1675.

Ullah, M., Pelletier, N., Xiao, L., Zhao, S.P., Wang, K., Degerny, C., Tahmasebi, S., Cayrou, C., Doyon, Y., Goh, S.L., et al., 2008. Molecular architecture of quartet MOZ/MORF histone acetyltransferase complexes. Mol. Cell. Biol. 28, 6828–6843.

van Eeden, F.J., Granato, M., Odenthal, J., Haffter, P., 1999. Developmental mutant screens in the zebrafish. Methods Cell. Biol. 60, 21–41.

Please cite this article as: Hibiya, K., et al., Brpf1, a subunit of the MOZ histone acetyl transferase complex, maintains expression of anterior and posterior *Hox* genes for prope... Dev. Biol. (2009), doi:10.1016/j.ydbio.2009.02.021

Wellik, D.M., 2007. Hox patterning of the vertebrate axial skeleton. Dev. Dyn. 236, 2454–2463.
Wellik, D.M., Capecchi, M.R., 2003. *Hox10* and *Hox11* genes are required to globally pattern the mammalian skeleton. Science 301, 363–367.
Willett, C.E., Zapata, A.G., Hopkins, N., Steiner, L.A., 1997. Expression of zebrafish rag genes during early development identifies the thymus. Dev. Biol. 182, 331–341.
Yang, X.J., 2004. Lysine acetylation and the bromodomain: a new partnership for signaling. Bioessays 26, 1076–1087.
Yang, X.J., Ullah, M., 2007. MOZ and MORF, two large MYSTic HATs in normal and cancer stem cells. Oncogene 26, 5408–5419.
Yu, B.D., Hanson, R.D., Hess, J.L., Horning, S.E., Korsmeyer, S.J., 1998. MLL, a mammalian trithorax-group gene, functions as a transcriptional maintenance factor in morphogenesis. Proc. Natl. Acad. Sci. U. S. A. 95, 10632–10636.
Yu, B.D., Hess, J.L., Horning, S.E., Brown, G.A., Korsmeyer, S.J., 1995. Altered Hox expression and segmental identity in Mll-mutant mice. Nature 378, 505–508.

Please cite this article as: Hibiya, K., et al., Brpf1, a subunit of the MOZ histone acetyl transferase complex, maintains expression of anterior and posterior *Hox* genes for prope.... Dev. Biol. (2009), doi:10.1016/j.ydbio.2009.02.021

Supplemental Material can be found at:
http://www.jbc.org/cgi/content/full/M805101200/DC1

THE JOURNAL OF BIOLOGICAL CHEMISTRY VOL. 284, NO. 1, pp. 237–244, January 2, 2009

Monocytic Leukemia Zinc Finger (MOZ) Interacts with p53 to Induce p21 Expression and Cell-cycle Arrest*[S]

Received for publication, July 7, 2008, and in revised form, October 27, 2008 Published, JBC Papers in Press, November 10, 2008, DOI 10.1074/jbc.M805101200

Susumu Rokudai[‡], Yukiko Aikawa[‡], Yusuke Tagata[‡], Nobuo Tsuchida[§], Yoichi Taya[¶], and Issay Kitabayashi[‡1]

From the [‡]Molecular Oncology Division, [¶]Radiobiology Division, National Cancer Center Research Institute, Tokyo 104-0045 and the [§]Department of Molecular Cellular Oncology and Microbiology, Tokyo Medical and Dental University, Tokyo 113-8510, Japan

Upon DNA damage, p53 can induce either cell-cycle arrest or apoptosis. Here we show that monocytic leukemia zinc finger (MOZ) forms a complex with p53 to induce p21 expression and cell-cycle arrest. The levels of the p53-MOZ complex increased in response to DNA damage to levels that induce cell-cycle arrest. $MOZ^{-/-}$ mouse embryonic fibroblasts failed to arrest in G_1 in response to DNA damage, and DNA damage-induced expression of p21 was impaired in $MOZ^{-/-}$ cells. These results suggest that MOZ is involved in regulating cell-cycle arrest in the G_1 phase. Screening of tumor-associated p53 mutants demonstrated that the G279E mutation in p53 disrupts interactions between p53 and MOZ, but does not affect the DNA binding activity of p53. The leukemia-associated MOZ-CBP fusion protein inhibits p53-mediated transcription. These results suggest that inhibition of p53/MOZ-mediated transcription is involved in tumor pathogenesis and leukemogenesis.

p53 is an important component of pathways mediating cellular responses to different forms of stresses, and induces expression of numerous target genes that regulate diverse cellular processes including cell-cycle arrest, apoptosis, and genome stabilization (1, 2). Many p53-targeted genes involved in cell-cycle arrest or apoptosis have been identified, including p21 (3), Bax (4), and Puma (5). Regulation of p53 transcriptional activity is essential for cellular responses to genotoxic stress, because p53 responds to DNA damage or checkpoint failure either by arresting the cell cycle in the G_1 phase for damage repair or by initiating an apoptotic pathway to eliminate the damaged cell (6–9). Several factors, such as TIP60, Hzf, and hCAS/CSE1L are involved in the selection of p53 target genes (10–13). However, the molecular mechanisms by which p53 chooses cell-cycle arrest *versus* apoptosis are not fully understood.

The principal post-translational modifications of p53 in response to DNA damage are phosphorylation and acetylation (14–17). Phosphorylation of Ser^{15} and Ser^{20} stabilizes p53 (16, 18, 19). Modification of p53 may also control the interactions of p53 with basal transcription factors (20), mediators (21), or coactivators, including histone acetyltransferases (HATs).[2] p53 interacts with components of several different HAT complexes, including p300/CBP (18), P/CAF (22), GCN5 (23), TRRAP (24), and TIP60 (11, 13). Additionally, p53-mediated transactivation of p21 correlates with increased histone acetylation (25). These results suggest that selective interactions between p53 and HATs may regulate target gene expression in response to diverse signals.

The monocytic leukemia zinc finger protein (MOZ) is a MYST-type HAT and functions as a co-activator of the AML1 transcription factor (8, 27). MOZ is involved in leukemia-associated chromosome rearrangements such as t(8;16)(p11;p13) (26), t(8;22) (27, 28), and inv(8) (29, 30), which result in fusion of MOZ to the transcriptional co-activators CBP, p300, and TIF2, respectively. Although MOZ and p300/CBP act as co-activators for AML1, MOZ-CBP inhibits AML1-mediated transcription (28, 31, 32). MOZ is essential for self-renewal of hematopoietic stem cells (33, 34). The MOZ-TIF2 fusion induces acute myeloid leukemia in irradiated recipient mice after transplantation (35, 36). MOZ-TIF2 also inhibits transcription by nuclear receptors and p53 by impairment of CBP function (37).

In this report, we demonstrate that MOZ directly interacts with p53. The level of the p53-MOZ complex increases after DNA damage, contributing to cell-cycle arrest in the G_1 phase.

EXPERIMENTAL PROCEDURES

Plasmids—cDNAs encoding FLAG-tagged or HA-tagged human *MOZ*, *CBP*, *MOZ-CBP*, and *AML1* were cloned into the pLNCX retroviral mammalian expression vector, as previously described (32). The sequences of the above constructs were checked by DNA sequencing. N- and C-terminal deletion mutants of *MOZ* cDNAs were generated by PCR with human wild-type *MOZ* as the template. The PCR-amplified deletion *MOZ* fragments were cloned into the HA-tagged pcDNA3.1(+) vector (Invitrogen). S15A, S15D, S20A, S20D, S46A, S46D, K382R, and K382Q mutants of p53 were derived from FLAG-tagged *p53*-pLNCX by site-directed mutagenesis using a QuikChange Site-directed Mutagenesis Kit (Stratagene).

* This work was supported by Grants-in-aid for Scientific Research from the Ministry of Health, Labor and Welfare, the Ministry of Education, Culture, Sports, Science and Technology, and the Program for Promotion of Fundamental Studies from the National Institute of Biomedical Innovation of Japan. The costs of publication of this article were defrayed in part by the payment of page charges. This article must therefore be hereby marked "*advertisement*" in accordance with 18 U.S.C. Section 1734 solely to indicate this fact.

[S] The on-line version of this article (available at http://www.jbc.org) contains supplemental Figs. S1–S4.

[1] To whom correspondence should be addressed: 5-1-1 Tsukiji, Chuo-ku, Tokyo 104-0045, Japan. Fax: 81-3-3542-0688; E-mail: ikitabay@ncc.go.jp.

[2] The abbreviations used are: HATs, histone acetyltransferases; MEFs, mouse embryonic fibroblasts; MOZ, monocytic leukemia zinc finger; ChIP, chromatin immunoprecipitation; HA, hemagglutinin; IP, immunoprecipitation; GST, glutathione *S*-transferase; RT, reverse transcriptase; ADR, adriamycin; siRNA, small interfering RNA; LC/MS, light chromatography/mass spectrometry.

Cells—Wild-type and MOZ$^{-/-}$ mouse embryonic fibroblasts (MEFs) were prepared from E13.5 embryos and cultured in Dulbecco's modified Eagle's medium with 10% fetal bovine serum in the presence of β-mercaptoethanol. Bosc 23 and Saos-2 cells were cultured as previously described (32).

Purification of the MOZ Complex and Mass Spectrometry—Bosc 23 cells were transiently transfected with FLAG-*MOZ*-pLNCX by using the calcium phosphate precipitation method. Transfected cells (1×10^{10}) were solubilized by incubation at 4 °C for 30 min in 50 ml of lysis buffer (20 mM sodium phosphate, pH 7.0, 250 mM NaCl, 30 mM sodium pyrophosphate, 0.1% Nonidet P-40, 5 mM EDTA, 10 mM sodium fluoride, 0.1 mM Na_3VO_4, and 1 mM phenylmethylsulfonyl fluoride) supplemented with protease inhibitors (Complete, Roche). The lysates were cleared by centrifugation at 30,000 × *g* for 30 min at 4 °C and incubated with 2.5 ml of anti-FLAG monoclonal antibody (M2)-conjugated affinity beads with rotation at 4 °C for 4 h. The beads were washed eight times, each with 50 ml of lysis buffer. The MOZ complexes were selectively eluted by incubating with 0.2 mg/ml FLAG peptide in lysis buffer for 1 h. The eluates were concentrated and separated using 10% SDS-PAGE. Proteins were stained with Coomassie Brilliant Blue, excised, destained with 25 mM ammonium bicarbonate and 50% acetonitrile, dried, digested with sequence grade modified trypsin (Promega) in 50 mM Tris (pH 7.6), extracted with 5% trifluoroacetic acid and 50% acetonitrile, and subjected to LC/MS/MS analysis. LC/MS/MS analysis was performed as previously described (32).

Immunoprecipitation and Immunoblot Analysis—Immunoprecipitation (IP) and immunoblot analyses were performed as previously described (38). In short, cells were solubilized with lysis buffer as described above, and sonicated 6 times for 10 s using a BioRuptor (Cosmo Bio) at the high power setting. Cell lysates were incubated with anti-FLAG monoclonal antibody (M2)-conjugated affinity beads (Sigma) for 4 h at 4 °C. The beads were washed five times with lysis buffer, and immunoprecipitates were selectively eluted by incubating with 0.2 mg/ml FLAG peptide in lysis buffer for 1 h. The eluates were concentrated and separated by SDS-PAGE. The rabbit polyclonal antibody to MOZ has been described previously (28). Commercially purchased antibodies to human p53 (DO-1), p21 (Santa Cruz Biotechnology), phospho-p53 (Ser^{15}, 16G8), phospho-p53 (Ser^{20}), phospho-p53 (Ser^{46}), FLAG M2, β-actin (Sigma), HA (3F10) (Roche), and mouse p53 (Ab-1) (Calbiochem) were also used in this study.

GST Pull-down Assays—For GST pull-down assays, *in vitro* translated products were generated using the TNT Quick Coupled System (Promega). *In vitro* translated [^{35}S]methionine-labeled N- and C-terminal deletion mutants of MOZ were incubated in the presence or absence of GST-tagged p53 and in the presence of glutathione-Sepharose 4B (Amersham Biosciences) in IP buffer overnight at 4 °C. The affinity beads were washed five times with IP buffer. The precipitates were subsequently resolved by SDS-PAGE and the [^{35}S]methionine-labeled proteins visualized by autoradiography (BAS2000, FUJIX).

Flow Cytometry—For flow cytometry analysis, cells were first fixed with 70% ethanol and then incubated with RNase A at 37 °C for 30 min. The cells were stained with propidium iodide (50 μg/ml propidium iodide in 0.1% sodium citrate and 0.1% Nonidet P-40) for 30 min at 4 °C. The cells were then analyzed using a FACS Calibur instrument (BD Biosciences) and Cell Quest software.

Luciferase Assays—Saos-2 cells were transfected in 24-well plates using the calcium phosphate precipitation method, and luciferase activity was assayed after 24 h using a luminometer (Veritas Microplate Luminometer, Turner Biosystems), according to the manufacturer's protocol (Promega). The results presented are the mean ± S.D. of relative luciferase activity generated from three independent experiments normalized against the activity of the internal control enzyme from pRL-CMV.

Semiquantitative RT-PCR Analysis—Total RNA was extracted using an RNeasy Mini Kit (Qiagen) according to the manufacturer's instructions. RT-PCR experiments were carried out with cDNAs generated from 2 μg of total RNA using a GeneAmp RNA PCR Kit (Applied Biosystems). The RT-PCR exponential phase was determined from 30 cycles of amplification to allow semiquantitative comparisons of cDNAs developed from identical reactions. All reactions involved initial denaturation at 95 °C for 5 min followed by 30 cycles of 95 °C for 30 s, 60 °C for 30 s, and 72 °C for 1 min using a GeneAmp PCR System 9700 (Applied Biosystems). Primers used in the RT-PCR study were as follows: mouse *p21*, 5′-CCGCACAGGAGCAAAGTGTG-3′ and 5′-GAATCTTCAGGCCGCTCAGAC-3′; mouse *Bax*, 5′-GCTGATGGCAACTTCAACTG-3′ and 5′-CACAAAGATGGTCACTGTCTG-3′; mouse *Mdm2*, 5′-CCTGTCCCAGGAGAGTGAC-3′ and 5′-GATTGGCTGTCTGCACACTG-3′; mouse *Puma*, 5′-GAGCCAAACCTGACCACTAG-3′ and 5′-GTGGTCACACGTGCTCTCTC-3′; control *glyceraldehyde-3-phosphate dehydrogenase*, 5′-CTTCACCACCATGGAGAAGGC-3′ and 5′-GGCATGGACTGTGGTCATGAG-3′.

DNA Binding Assay—Nuclear extracts were prepared from Bosc 23 cells 24 h after transfection with wild-type or mutant *p53*. Procedures for DNA binding reactions were similar to those previously described (39). Briefly, reaction mixtures contained 4 μg of extract in 18 μl of binding buffer (50 mM KCl, 20 mM HEPES, pH 7.5, 10 mM $MgCl_2$, 10% glycerol, 0.5 mM dithiothreitol, 0.1% Nonidet P-40), plus 1 μg of sonicated DNA from salmon testes. The double-stranded *p21* oligonucleotide probe 5′-GTCAGGAACATGTCCCAACATGTTGAGCTC-3′ was derived from the p21^{Waf1} promoter. Reaction mixtures were incubated for 15–20 min at 23 °C with the addition of 1 ng of radiolabeled probe. Each reaction mixture was then loaded onto a native 4% polyacrylamide gel (acrylamide:Bis, 50:1; 0.5 × TBE) and electrophoresed in 0.25 × TBE at 180–220 V for 3 h at 4 °C.

ChIP Assays—MCF-7 cells were fixed directly by adding 270 μl of 37% formaldehyde to 10 ml of culture medium and incubated at 37 °C for 10 min. The fixed cells were harvested and prepared for immunoprecipitation using a chromatin immunoprecipitation assay kit (Upstate Biotechnology), according to the manufacturer's instructions. In brief, the lysates were precleared with salmon sperm DNA-protein A-agarose, and subsequently incubated with 1 μg of anti-p53 antibody (DO-1)

(Santa Cruz), anti-MOZ antibody, or control IgG at 4 °C overnight. Samples were washed with low salt buffer, high salt buffer, once with LiCl, and twice with TE. Immune complexes were eluted (cross-links reversed), and then purified using a PCR purification kit (Qiagen). Samples (5 μl) were subjected to PCR amplification. The PCR were carried out with Pfu Turbo DNA Polymerase (Stratagene).

All reactions involved initial denaturation at 95 °C for 5 min followed by 35 cycles of 95 °C for 30 s, 60 °C for 30 s, and 72 °C for 1 min using a GeneAmp PCR System 9700 (Applied Biosystems). The PCR primers used were as follows: *p21*RE1, 5′-CAGGCTGTGGCTCTGATTGG-3′ and 5′-TTCAGAGTAACAGGCTAAGG-3′; *p21*RE2, 5′-GGTCTGCTACTGTGTCCTCC-3′ and 5′-CATCTGAACAGAAATCCCAC-3′; *p21* (−1808), 5′-CTTAAGAAATATTGAATGTCG-3′ and 5′-CTAGACATTGTCTGTCTG-3′; *mdm2*, 5′-TGGGCAGGTTGACTCAGCTTTTCCTC-3′ and 5′-TTCCGAAGCTGGAATCTGTGAGGTGG-3′; *bax*, 5′-CAGCGCTTTGGAAGGCTGAGAC-3′ and 5′-GTGACTGTCCAATGAGCATCTC-3′; and *puma*, 5′-GAGACTGTGGCCTTGTGTC-3′ and 5′-GGACAAGTCAGGACTTGCAG-3′.

Cytotoxicity Assays—Wild-type (WT), MOZ$^{-/-}$, and p53$^{-/-}$ MEF cells were plated in 96-well plates at a concentration of 1 × 10^4 cells in 100 μl of complete medium. After a 12-h incubation, MEF cells were treated with 0, 0.1, 0.5, 1, 5, or 10 μM adriamycin (ADR). After 36- or 48-h incubations, cell viability, based on mitochondrial succinate dehydrogenase activity, was measured using a Cell Counting Kit-8 (Dojin), which utilizes a WST-8 (2-[2-methoxy-4-nitrophenyl]-3-[4-nitrophenyl]-5-[2,4-disulfophenyl]-2*H*-tetrazolium, monosodium salt) assay. Data are presented as the mean ± S.D. of three independent experiments.

Antisense Oligonucleotides—To inhibit expression of endogenous MOZ, small interfering RNA (siRNA) duplex with a 3′ dTdT overhang corresponding to *MOZ* mRNA (AAGGAUAUGCAAUGCUGUGUC) was synthesized (Dharmacon). Nonspecific control siRNA (Dharmacon) was used as a negative control. Antisense oligonucleotides (200 nM) were transfected twice using Lipofectamine 2000 (Invitrogen).

RESULTS

Interaction between p53 and MOZ—To identify MOZ-interacting proteins, we purified MOZ complexes. The complexes of MOZ were partially purified using affinity beads conjugated with anti-FLAG M2 antibody (Fig. 1*A*). The MOZ-purified fraction contained multiple proteins that were absent from the mock-purified fraction, suggesting that they interact specifically with MOZ. To identify these proteins in the MOZ fraction, we analyzed these specific proteins using mass spectrometry analysis and found that the spectrum obtained from peptides was identified as p53, as well as BRPF1 (40), C23, HSP70, and B23 (Fig. 1*A*). Co-immunoprecipitation analysis confirmed that these putative associated proteins, including p53, were co-precipitated with MOZ (Fig. 1*B*). Reciprocal co-immunoprecipitation showed that MOZ was co-precipitated with p53 (Fig. 1*C*).

Interacting Domains on p53 and MOZ—To determine the p53-interacting domains of MOZ, the interaction between MOZ and p53 was examined by IP immunoblot analysis using

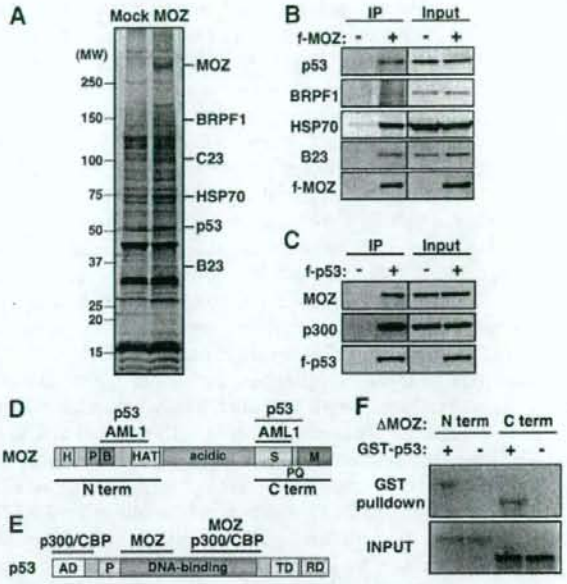

FIGURE 1. **MOZ interacts with p53.** *A*, FLAG-tagged MOZ proteins were partially purified from lysates of cells transfected with either mock (*Mock*) or FLAG-tagged MOZ (*MOZ*) using anti-FLAG M2 affinity beads. The eluates were concentrated and separated by SDS-PAGE. Gels were silver-stained to detect proteins. *B*, the fractions in *A* were analyzed by immunoblot analysis using antibodies against p53, BRPF, HSP27, B23, or FLAG. *C*, FLAG-tagged p53 was immunoprecipitated from cell lysates using anti-FLAG M2 affinity beads. The precipitates were analyzed by immunoblot analysis using anti-MOZ or anti-p300 (*left*) antibodies. Input lysate samples were subjected to immunoblot analysis (*right*). *D*, p53 interacts with two regions of MOZ (see supplemental Fig. S1). *E*, MOZ interacts with the DNA binding domain of p53 (see supplemental Fig. S2). *F*, p53 interacts directly with either the N or C terminus of MOZ. A GST pull-down assay was performed using GST-tagged p53 protein in the presence of *in vitro* translated [^{35}S]methionine-labeled N- or C-terminal fragments of MOZ (see *D*).

deletion mutants of MOZ. Bosc 23 cells, which exhibit very high transfection efficiency, were transfected with FLAG-tagged p53 and HA-tagged wild-type or mutant MOZ. The expression of MOZ mutants and results of the IP immunoblot analysis are shown in supplemental Fig. S1, and summarized in Fig. 1*D*. These results suggest that there are at least two p53-interacting domains in MOZ, one lies in the basic domain between amino acids 312 and 664, and another lies in the serine-rich domain between amino acids 1517 and 1741. Similarly, to determine the region of p53 required for binding to MOZ, IP immunoblot analysis was conducted using a series of p53 deletion mutants. Each of the p53 mutants was immunoprecipitated by using anti-FLAG antibody M2 (supplemental Fig. S2), and the results are summarized in Fig. 1*E*. These results suggest that the p53-core DNA binding domain (amino acids 98–180 and 202–296) is required for its interaction with MOZ. To further examine whether these interactions are direct or indirect, we performed *in vitro* GST pull-down assays, and showed that either the N or C terminus of MOZ could interact directly with p53 *in vitro* (Fig. 1*F*).

Impaired G_1 Arrest in MOZ$^{-/-}$ Cells—To investigate the role of MOZ in DNA damage responses, we tested the effects of ADR on cell cycle progression in wild-type and MOZ$^{-/-}$ MEFs. Analysis by flow cytometry showed that wild-type cells were

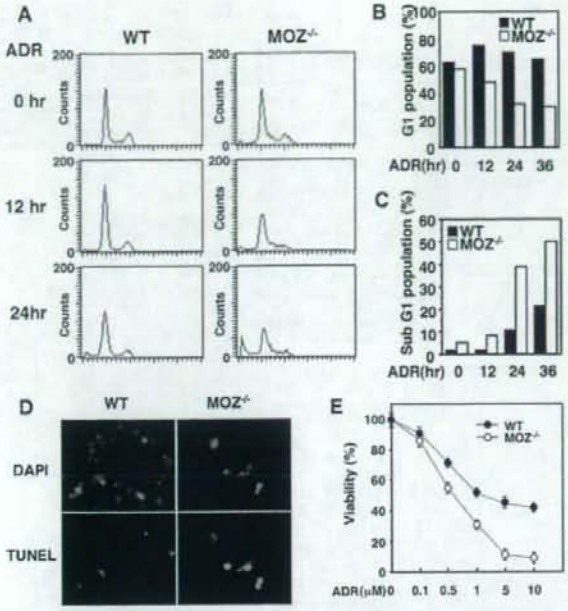

FIGURE 2. **MOZ-deficient cells fail to arrest in G_1 phase in response to DNA damage.** *A*, induction of G_1 arrest after ADR treatment in wild-type (*WT*) MEFs, but not $MOZ^{-/-}$ MEFs. FACS analysis at the indicated times after 5 μM ADR treatment of WT and $MOZ^{-/-}$ MEF cells. *B* and *C*, the percentages of (*B*) G_1 and (*C*) sub-G_1 cells in *A* were quantified. *D*, $MOZ^{-/-}$ MEF cells are sensitive to ADR. The panel shows representative photographs of WT or $MOZ^{-/-}$ MEFs at 36 h following 5 μM ADR treatment. Apoptosis was detected by TUNEL. *E*, cytotoxicity of ADR treatment in WT or $MOZ^{-/-}$ MEF cells. MEFs were incubated with the indicated concentrations of ADR for 36 h. Cell viability was measured using a Cell Counting Kit-8, which is a WST-8 assay. *DAPI*, 4′,6-diamidino-2-phenylindole.

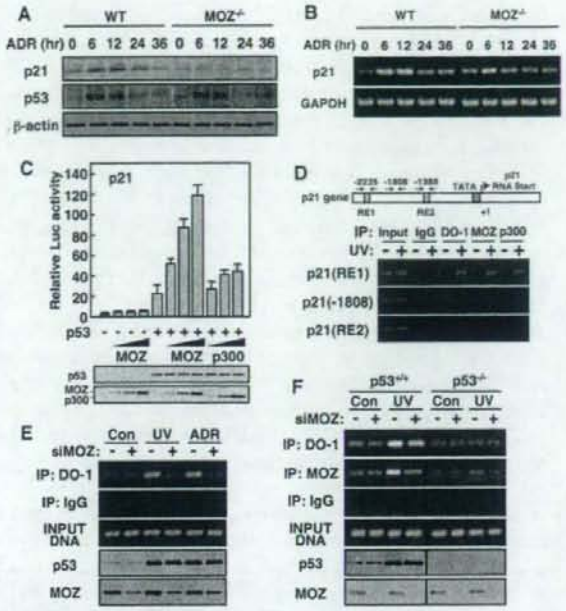

FIGURE 3. **MOZ activates p53-mediated transcription of p21.** *A*, impaired p21 expression in MOZ knock-out cells. Expression of p53 and p21 at the indicated times following 5 μM ADR treatment in wild-type (*WT*) or $MOZ^{-/-}$ MEF cells. Cell lysates were analyzed by immunoblot analysis using anti-p21, anti-p53, or anti-β-actin (loading control) antibodies. *B*, impaired p21 induction in MOZ knock-out cells. Induction of p21 and β-actin at the indicated times following 5 μM ADR treatment in WT or $MOZ^{-/-}$ MEF cells. RT-PCR analysis was performed as described under "Experimental Procedures." *C*, effects of MOZ and p300 on p53 activity. Saos-2 cells were transfected with 50 ng of p21-luc, 10 ng of pLNCX-*p53* (*lanes 5–11*), and 30 (*lanes 2, 6*, and *9*), 100 (*lanes 3, 7*, and *10*), or 350 ng (*lanes 4, 8*, and *11*) of pLNCX-*MOZ* (*lanes 2–4* and *6–8*), or pLNCX-p300 (*lanes 9–11*) and pRL-CMV. Luciferase assays were performed 24 h post-transfection. The expression levels of transfected p53 and MOZ/p300 are shown *below* in *C*. *D*, ChIP assays were performed to assess the co-association of p53, MOZ, and p300 at different *p21* promoter regions 12 h after 30 J/m² UV irradiation (*lanes 2, 4, 6, 8*, and *10*) in MCF-7 cells. Cell extracts were subjected to ChIP assays with anti-p53 (*DO-1*, *lanes 5* and *6*), anti-MOZ (*lanes 7* and *8*), or anti-p300 (*lanes 9* and *10*), as well as an IgG control (*lanes 3* and *4*). Precipitates were analyzed by PCR using the indicated p21 promoter primers shown at the *top* of the panel. *E*, ChIP assay at the *p21*RE1 promoter region in wild-type or MOZ knockdown cells. MCF-7 cells were transfected twice with either control siRNA or MOZ siRNA. At 36 h post-transfection, the cells were treated either with 30 J/m² of UV radiation or 5 μM ADR. After 12 h the cell extracts were subjected to ChIP assay with anti-p53 antibody (*IP: DO-1*) as well as IgG control (*IP: IgG*). Immunoprecipitated and input DNA (*INPUT DNA*) were then subjected to RT-PCR analysis using p21RE1 promoter primer. Input lysates were partially subjected to immunoblot analysis using anti-p53 or anti-MOZ antibodies (*lower panels*). *F*, ChIP assay at the *p21*RE1 promoter region in wild-type ($p53^{+/+}$) or p53-depleted ($p53^{-/-}$) HCT-116 cells. The cells were transfected twice with either control siRNA or MOZ siRNA. At 36 h post-transfection, the cells were treated with (*UV*) or without (*Con*) 30 J/m² of UV radiation. After 12 h, the cell extracts were subjected to ChIP assay with anti-p53 (IP: *DO-1*) or anti-MOZ (IP: *MOZ*) antibodies as well as IgG control (IP: *IgG*). Immunoprecipitated and input DNA (*INPUT DNA*) were then subjected to RT-PCR analysis using *p21*RE1 promoter primer. Input lysates were partially subjected to immunoblot analysis using anti-p53 or anti-MOZ antibodies (*lower panels*).

arrested in the G_1 phase of the cell cycle, and that the number of cells in G_1 peaked 12 h after ADR treatment (Fig. 2, *A* and *B*). However, in MOZ-deficient cells, the number of cells in the G_1 phase decreased after ADR treatment, and the number of apoptotic cells in the sub-G_1 phase increased (Fig. 2, *A* and *C*). These differences in sensitivity to ADR-induced DNA damage were also observed in TUNEL assays (Fig. 2*D*) and in cytotoxicity assays (Fig. 2*E*). These results suggest that in response to DNA damage, MOZ-deficient cells failed to arrest in G_1 phase and tended to undergo apoptosis.

Impaired Expression of the p21 Gene in $MOZ^{-/-}$ Cells—The altered response of $MOZ^{-/-}$ MEFs to DNA damage suggests that the p53 pathway might be altered in $MOZ^{-/-}$ MEFs. To test this hypothesis, we examined the expression of the p53 target gene *p21* after ADR treatment. In wild-type MEFs, *p21* expression increased after ADR treatment in a dose-dependent manner and reached a maximum at 6–12 h (Fig. 3, *A* and *B*, supplemental Fig. S3, *A–C*). However, expression and induction of *p21* were profoundly impaired in $MOZ^{-/-}$ MEFs as assessed by immunoblot analysis, Northern blotting, and real-time RT-PCR analyses. Furthermore, expression of the other p53 target genes, such as *Mdm2*, *Bax*, and *Puma*, were induced by ADR treatment both in wild-type and $MOZ^{-/-}$ cells (supplemental Fig. S3, *D* and *E*). Thus, these results suggested that MOZ is required for p53-induced expression of *p21*, but not for those of *Bax*, *Mdm2*, and *Puma*.

MOZ Induces the Expression of the p21 Gene—To test whether MOZ directly affects p53-mediated transcription, we used reporter plasmids under the control of p21 promoters. MOZ strongly stimulated p53-mediated activation of p21-luc rather than p300 (Fig. 3*C*). However, BAX-luc and AIP1-luc were activated by p300 but not by MOZ (supplemental Fig. S3, *F* and *G*). ChIP assays showed that after UV radiation, MOZ